NEW TECHNIQUES TO DESIGN PERFORMANCE IMPROVED POWER DIVIDERS AND DIRECTIONAL COUPLERS USING THE NEW SCATTERING PARAMETER RELATIONS

A DISSERTATION SUBMITTED TO

THE GRADUATE SCHOOL OF ENGINEERING AND SCIENCE

OF BILKENT UNIVERSITY

IN PARTIAL FULFILLMENT OF THE REQUIREMENTS FOR

THE DEGREE OF

DOCTOR OF PHILOSOPHY

IN

ELECTRICAL AND ELECTRONICS ENGINEERING

By

Vahdettin Taş

February, 2015

NEW TECHNIQUES TO DESIGN PERFORMANCE IMPROVED POWER DIVIDERS AND DIRECTIONAL COUPLERS USING THE NEW SCATTERING PARAMETER RELATIONS

By Vahdettin Taş

February, 2015

We certify that we have read this thesis and that in our opinion it is fully adequate, in scope and in quality, as a dissertation for the degree of Doctor of Philosophy.

Prof. Dr. Abdullah Atalar(Advisor)

Prof. Dr. Şimşek Demir

Assoc. Prof. Dr. Vakur B. Ertürk

Prof. Dr. Ayhan Altintas

Assoc. Prof. Dr. Arif Sanli Ergun

Approved for the Graduate School of Engineering and Science:

Prof. Dr. Levent Onural
Director of the Graduate School

ABSTRACT

NEW TECHNIQUES TO DESIGN PERFORMANCE IMPROVED POWER DIVIDERS AND DIRECTIONAL COUPLERS USING THE NEW SCATTERING PARAMETER RELATIONS

Vahdettin Taş
Ph.D. in Electrical and Electronics Engineering
Advisor: Prof. Dr. Abdullah Atalar
February, 2015

Wide bandwidth provides with several benefits in RF applications such as enabling high data rates for communication applications, enhancing the multi tread avoiding capabilities of the jamming systems, improving the effectiveness of spread spectrum techniques. Operation in a wide bandwidth requires either broadband components or multiple narrow band components together with sophisticated multiplexing methods. There are several trivial methods to increase the bandwidth of the RF components. For instance the bandwidth of a power divider can be increased by increasing the number of sections which directly increases the insertion loss and circuit size, burdening a big trade off for the designer. The methods avoiding such a trade off are life savers in most of the applications. Such methods require new design approaches. This work aims to develop such methods with a special focus on improving the bandwidth and performance of the power dividers and directional couplers. We derive new scattering parameter relations and show that the relations require tricky design guidelines. S-parameter relations for a number of power divider types and directional coupler schemes are investigated. The derived equations have significant usages. One of the equations is used to design the optimal isolation network for the Wilkinson power divider. A number of equations imply a reduction in the number of the optimization parameters in the design of n-section or n-way dividers. Another equation is used to increase the directivity of microstrip directional couplers in a wide bandwidth. Experimental results are presented verifying the theoretical work.

Keywords: Scattering parameters, Wilkinson divider, wideband power divider, isolation network, even mode, odd mode, reflection coefficients, coupler phase relations, coupling isolation phase difference, high directivity.

ÖZET

YENİ SAÇILIM PARAMETRESİ İLİŞKİLERİNİ KULLANARAK PERFORMANSI GELİŞTİRİLMİŞ GÜÇ BÖLÜCÜLER VE YÖNLÜ BAĞLAÇLAR TASARLAMAK İÇİN YENİ TEKNİKLER

Vahdettin Taş
Elektrik-Elektronik Mühendisliği, Doktora
Tez Danışmanı: Prof. Dr. Abdullah Atalar
Şubat, 2015

Geniş bant aralığı, iletişim uygulamalarında yüksek veri hızına olanak sağlaması, sinyal karıştırma uygulamalarında çoklu tehditleri engelleme yeteneğinin artırılması, yayılı spektrum tekniklerinde etkinliğinin yükseltilmesi gibi çeşitli avantajlarla RF uygulamalara yarar sağlamaktadır. Geniş bir bant aralığında operasyon, geniş bantlı bileşenlere ya da karmaşık çoklama teknikleriyle birlikte çoklu sayıda dar bantlı bileşenlere gereksinim duyurmaktadır. RF bileşenlerin bant genişliğini artırmak için açık yöntemler mevcuttur. Örnek olarak, bir güç bölücünün bant genişliği kısım sayısının artırılmasıyla artırılabilir, bu çözüm güç kaybına ve boyut büyümesine sebep olarak tasarımcıyı bir ikileme sürmektedir. İkilemsiz çözüm sağlayan metotlar birçok uygulamada kritik öneme sahiptir. Bu metotlar yeni tasarım yaklaşımları gerektirmektedirler. Bu çalışma söz konusu metotları geliştirmeyi amaçlamakta özellikle güç bölücülerin ve yönlü bağlaçların bant genişliğini ve performanslarını artırmayı hedeflemektedir. Çeşitli güç bölücü türleri ve yönlü bağlaç yapıları için yeni saçılım parametreleri ilişkilerini araştırmış bulunuyoruz. Türetilen denklemlerin kritik kullanımları ortaya çıkmıştır. Bir denklem Wilkinson bölücüsü için optimum izolasyon devresinin tasarımında kullanılmıştır. Bazı denklemeler n-kısımlı veya n-yollu güç bölücülerin tasarımında ihtiyaç duyulan optimizasyon parametrelerinin sayılarının azaltılabileceğini ortaya koymuştur. Bir başka denklem, mikroşerit bağlaçların yönlülük parametresini geniş bir bant aralığında artırmakta kullanılmıştır. Teorik çalışmaları destekleyici deneysel sonuçlar sunulmaktadır.

Anahtar sözcükler: Saçılım parametreleri, Wilkinson bölücüsü, geniş bantlı güç bölücü, izolasyon devresi, eş mod, zıt mod, yansıma katsayısı, baglaç faz ilişkileri, bağlaşim izolasyon faz farkı, yüksek yönlülük.

Acknowledgement

I am grateful to Prof. Abdullah Atalar for his guidance throughout my MS and PhD studies. Prof. Atalar's broad vision and knowledge will always inspire me in my future works.

I would like to thank Prof. Simsek Demir and Prof. Vakur B. Erturk for their helpful comments in our research meetings. I am thankful to the other members of my dissertation committee Prof. Ayhan Altintas and Prof. Arif Sanli Ergun for their careful reading of the dissertation draft and helpful suggestions.

I would like to thank to the members of the Power Amplifier Technologies Division at ASELSAN Inc. for their assistance in my works. I am especially grateful to Necip Sahan, Hakan Korkmaz, Cagri Balikci and our manager Ahmet Kirlilar. I am thankful to Irfan Yildiz and Sami Altan Hazneci from METEKSAN Defense Inc. for assisting me with the tricky practical aspects of RF design in my first years of RF engineering.

I am thankful to the members of Prof. Atalar's research group for joyful discussions in our research meetings. Akif Alperen Coskun, Ceyhun Kelleci, Okan Unlu, Sinan Alemdar and Kenan Ozel are gratefully acknowledged. I would like to memorialize our former colleague Deniz Aksoy, he was an extraordinary person with a brilliant mind.

I am thankful to TUBITAK for providing me financial supports throughout my MS and PhD studies.

Finally, I would like to express my gratitude to my family, my mother Gulseren Tas , my father Arslan Tas, my beloved wife Betul and our new member Ahmet Arslan.

Contents

List of Figures

List of Tables

Chapter 1

Introduction

The even-odd mode decomposition technique introduced by Reed and Wheeler [2] is the common technique to analyze microwave devices whenever applicable. Various kinds of power dividers are analyzed using this method and their Scattering parameters (S-parameters) have been well formulated. However, the relations between the S-parameters needs more exploration as they can require tricky design guidelines. In this work, we derive new S-parameter relations for various kinds of power dividers and directional couplers. The analysis are based on symmetry arguments, energy arguments, network theory and even/odd mode analysis techniques.

Power dividers are used at microwave frequencies to direct the power to two or more loads. Normally, they maintain the matched condition at all ports within the operation band. Moreover, a good isolation between the output ports is desired to eliminate the interaction between the loads. When used in the opposite direction, power dividers can combine power from two or more power sources. The Wilkinson power divider was introduced in 1960 [3]. Around the center frequency it is matched at all ports and isolated at the output ports within a relatively narrow bandwidth. Cohn [1] introduced the multisection hybrids to improve the operation bandwidth of the Wilkinson divider. Broadband power division using multisection structures was revealed in several studies [4–9]. Wide operation bandwidth is also achieved by utilizing tapered lines. They are constructed using a continuum of a long tapered line [10] or multisection tapered lines [11]. The main disadvantage of using multi sections is the increase in the length and the insertion loss of the divider. To avoid this, a number of researchers designed reduced size dividers [12–15]. Another approach to improve the bandwidth response of the Wilkinson divider aims dual band operation. This is achieved by using RLC networks in series or parallel configuration between the output ports [16–18], coupled lines [19], parallel stubs along the transmission path [20] and right-left handed transmission lines [21]. These designs also require an increase in length. Other works [22],[23] focus on the isolation network design for isolation bandwidth improvement. Length increment is avoided by modifying only the isolation network. In these works, the isolation bandwidth is widened while the input return loss is kept unchanged. Due to the position of the isolation resistors extra insertion loss is faced.

In Chapter-2, we derive S-parameter relations for various kinds of power dividers. Applications of these relations are explained. One of the equations is used in Chapter-3 to design the optimal isolation network for the Wilkinson divider. Our goal is to design an isolation network that improves the bandwidth of input return loss, output return loss and isolation, simultaneously. This way, the number of sections is not increased hence extra length and loss are avoided. We calculate the optimal reflection coefficients of the isolation network in the even mode and odd mode cases. Circuits are constructed to realize the calculated reflection coefficients. The resulting circuits are combined in the final divider structure. Detailed analytical work and simulation results for the single and two-section dividers are presented along with the experimental results.

Chapter-4 explores directivity and bandwidth performance of the microstrip directional couplers. Planar characteristic of the microstrip line technology offers substantial advantages with a low cost of fabrication and integrability with other components. The propagation mode in a microstrip line is quasi-TEM, because the medium is inhomogeneous. The quasi-TEM mode propagation is especially problematic when coupled line directional couplers are under consideration. The inhomogeneity of the medium causes the even and odd modes to propagate with different velocities that degrade directivity [24].

There are several methods to compensate the even-mode odd-mode velocity differences in microstrip line directional couplers. Podell [25] introduced the wiggly line coupler. In that design, the odd mode travels a longer path; hence it is slowed down relative to the even mode. Dielectric overlays [26, 27] achieves a velocity equalization as the overlay brings the quasi-TEM mode propagation closer to a pure TEM mode. Lumped element compensation is explored in several works [28–30]. Moderate bandwidth and directivity levels were achieved using these methods. A recent work [31] demonstrated a wideband compensation using interdigital capacitors. In another recent work [32] both high directivity and tight coupling were achieved by cascading couplers in a narrow bandwidth. High values of directivity improvement were obtained using voltage cancellation methods. In [33, 34] termination impedances were adjusted to cancel the transmission to the isolated port. Feedforward compensation was applied in [35, 36]. Bypass circuits were utilized in [37]. The techniques based on voltage cancellation [33–37] achieved high directivity values, however the frequency range of the directivity improvement was narrowband relative to the quarter wavelength frequency.

The phase relations between the coupled port and the isolated port have not been explored in the literature. To the authors' knowledge, there is only one reference [36] to a π phase difference for a quarter wavelength coupler design, but no analysis is presented about the frequency or dimensional dependence. Using even-odd mode analysis, we show that the phase difference between the coupling factor and the isolation factor is close to π from DC up to the half wavelength frequency [38]. Network analysis also yields that complex isolation factor and the coupling factor of a microstrip coupled line coupler lie along the same vector. This fact presents a high potential to achieve broadband directivity improvement through a voltage cancellation at the isolated port. We aim to obtain wide band high directivity by improving the voltage cancellation methods in the light of the new S-parameter phase relations. Two coupler architectures are investigated for improvement. Using the proposed method, the directivity bandwidth of couplers is significantly increased.

Chapter 2

S-Parameter Relations for Power Dividers

New equations are derived for various kinds of power dividers using symmetry, energy arguments and even/odd mode analysis. First, we consider lossless power dividers: symmetrical 2-way, n-way. The power dividers can have lumped or distributed elements. The S-parameter relations for this case relate the magnitude of some S-parameters. Then, we consider single or multisection 2-way, n-way and asymmetrical Wilkinson dividers built from transmission lines with optimum impedances. For the Wilkinson case, phases of the S-parameters are related in addition to the magnitudes.

2.1 Lossless Symmetrical 2-Way Divider

In Fig. 2.1, a symmetrical multisection 2-way divider network is shown. White and gray boxes can contain lossless and reciprocal lumped or distributed components as long as the symmetry between the two arms is maintained. Impedances of the output ports are allowed to differ from the input port impedance to generalize the results. S-parameter matrix equation of such a three port is given by

$$\begin{bmatrix} b_1 \\ b_2 \\ b_3 \end{bmatrix} = \begin{bmatrix} S_{11} & S_{21} & S_{21} \\ S_{21} & S_{22} & S_{32} \\ S_{21} & S_{32} & S_{22} \end{bmatrix} \begin{bmatrix} a_1 \\ a_2 \\ a_3 \end{bmatrix} \tag{2.1}$$

where $|a_n|^2$ and $|b_n|^2$ are the incident and reflected powers at port n. S_{21} can be represented with the following formula:

$$S_{21} = e^{-j\phi}\sqrt{\frac{1-|S_{11}|^2}{2}} \tag{2.2}$$

where a frequency dependent transmission phase of ϕ is assumed.

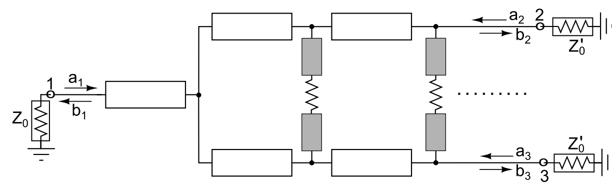

Figure 2.1: A symmetrical 2-way power combiner/divider network with a termination of Z_0 at port 1 and Z_0' at ports 2 and 3. White and gray boxes contain lossless lumped or distributed elements.

If $a_1 = 0$ and $a_2 = a_3 = 1/\sqrt{2}$ are applied, we find

$$b_1 = e^{-j\phi}\sqrt{1-|S_{11}|^2}, \quad b_2 = b_3 = \frac{S_{22}+S_{32}}{\sqrt{2}} \tag{2.3}$$

The incident power is $|a_2|^2 + |a_3|^2 = 1$. Due to the symmetry, there will be no loss in the isolation resistor, and the total incident power equals the transmitted power plus the total reflected power:

$$|a_2|^2 + |a_3|^2 = |b_1|^2 + |b_2|^2 + |b_3|^2 \tag{2.4}$$

From (2.3) and (2.4) we find

$$1 = |b_1|^2 + |b_2|^2 + |b_3|^2 = (1-|S_{11}|^2) + |S_{32}+S_{22}|^2 \tag{2.5}$$

and finally we arrive at the result

$$|S_{11}| = |S_{22}+S_{32}| \tag{2.6}$$

The result in (2.6) states that the magnitude of the input reflection coefficient equals the magnitude of the sum of the output reflection coefficient and isolation term. If any two of the three parameters are zero, the third one must be also zero.

2.2 Lossless Symmetrical n-Way Divider

The analysis above can be extended to n-way combiner/divider networks. For a symmetrical, reciprocal, lossless n-way combiner/divider with port 1 signifying the common port, we can write the S-parameters as

$$\begin{aligned} S_{ii} = S_{22} \;\text{ for }\; i = 3,..,n+1 \\ |S_{1i}| = \sqrt{\frac{1-|S_{11}|^2}{n}} \;\text{ for }\; i = 2,..,n+1 \\ S_{ij} = S_{32} \;\text{ for }\; i,j = 2,..,n+1 \;\text{ and }\; i \neq j \end{aligned} \tag{2.7}$$

We apply $a_1 = 0$ and $a_i = 1/\sqrt{n}$, $i = 2,..,n+1$, so that the input power is unity: $|a_2|^2 + |a_3|^2 + .. + |a_{n+1}|^2 = 1$. Under this condition we find

$$\begin{aligned} |b_1| &= \sqrt{1-|S_{11}|^2} \\ b_2 = b_3 = \ldots = b_{N+1} &= \frac{S_{22}+(n-1)S_{32}}{\sqrt{n}} \end{aligned} \tag{2.8}$$

Due to symmetry, there will be no loss in the isolation resistors and the total output power is also unity

$$|b_1|^2 + |b_2|^2 + .. + |b_{n+1}|^2 = 1 \tag{2.9}$$

Combining (2.8) and (2.9), we find

$$1 - |S_{11}|^2 + n\left|\frac{S_{22}+(n-1)S_{32}}{\sqrt{n}}\right|^2 = 1 \tag{2.10}$$

and arrive at the final result for symmetrical n-way dividers:

$$|S_{11}| = |S_{22} + (n-1)S_{32}| \tag{2.11}$$

If $|S_{22}| \ll (n-1)|S_{32}|$, then we have $|S_{11}| \approx (n-1)|S_{32}|$.

In some high power applications, the isolation resistors are not used for practical reasons. In such a power combiner, the input return loss can be made very large, while isolation and output return losses suffer. In that case, (2.11) predicts that

$$|S_{22} + (n-1)S_{32}| \approx 0 \quad\text{or}\quad S_{22} \approx -(n-1)S_{32} \tag{2.12}$$

Expressed in decibels, $S_{22dB} \approx S_{32dB} + 20\log(n-1)$. For example, for a 4-way divider, the isolation will be 9.5 dB better than the output return loss.

2.3 Reflection Coefficients of a Two Port Transmission Line Network

The derivation of the S-parameter relations for the Wilkinson type dividers requires the analysis of the reflection coefficients of the circuits composed of transmission lines with specific characteristic impedances.

2.3.1 Single section transmission line

Consider a lossy transmission line of length L. Its characteristic impedance is $Z_L = \sqrt{Z_{01}Z_{02}}$ and it is terminated with impedances of Z_{01} and Z_{02} at its terminals as indicated in Fig. 2.2. The input impedance at the port 1 is

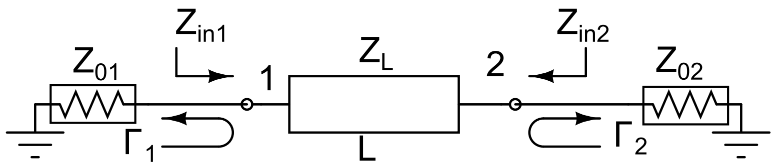

Figure 2.2: A transmission line with a characteristic impedance of $Z_L = \sqrt{Z_{01}Z_{02}}$ is terminated with impedances Z_{01} and Z_{02}.

$$Z_{in1} = Z_L \frac{Z_{02} + Z_L \tanh(\gamma L)}{Z_L + Z_{02} \tanh(\gamma L)} \tag{2.13}$$

where γ is the complex propagation constant. The reflection coefficient at this port, Γ_1, is given by

$$\Gamma_1 = \frac{Z_{in1} - Z_{01}}{Z_{in1} + Z_{01}} = \frac{Z_L(Z_{02} - Z_{01})}{Z_L(Z_{01} + Z_{02}) + 2Z_{01}Z_{02} \tanh(\gamma L)} \tag{2.14}$$

Similarly, the reflection coefficient at port 2 equals

$$\Gamma_2 = \frac{Z_{in2} - Z_{02}}{Z_{in2} + Z_{02}} = \frac{Z_L(Z_{01} - Z_{02})}{Z_L(Z_{01} + Z_{02}) + 2Z_{01}Z_{02} \tanh(\gamma L)} \tag{2.15}$$

Hence we find for this special case

$$\Gamma_1 = -\Gamma_2 \tag{2.16}$$

for all frequencies and independent of the transmission line length, L.

2.3.2 N-section transmission lines

Consider the transmission line structure shown in Fig. 2.3. Compared to Fig. 2.2, two more equal length lossy transmission lines are added. The characteristic impedances of Z_1 and Z_2 are chosen such that

$$Z_1 Z_2 = Z_{01} Z_{02} = Z_L^2 \tag{2.17}$$

The loss per unit electrical length should be the same for Z_1 and Z_2. Note that if $Z_1 = Z_{01}$, then $Z_2 = Z_{02}$ and the circuit reduces to the circuit in Fig. 2.2 apart from the additional phase shift, hence Eq. 2.16 holds.

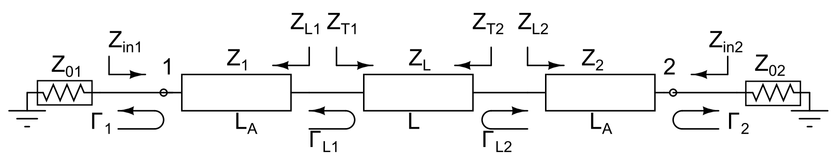

Figure 2.3: Three transmission lines terminated with impedances Z_{01} and Z_{02}. The transmission lines satisfy the relation $Z_L = \sqrt{Z_{01}Z_{02}}$, $Z_1 Z_2 = Z_{01}Z_{02}$. Z_1 and Z_2 have equal electrical lengths and equal losses.

With $Z_1 \neq Z_{01}$, the new impedances seen by Z_L are

$$\begin{aligned} Z_{L1} &= Z_1 \frac{Z_{01} + Z_1 \tanh(\gamma L_A)}{Z_1 + Z_{01}\tanh(\gamma L_A)} \\ Z_{L2} &= Z_2 \frac{Z_{02} + Z_2 \tanh(\gamma L_A)}{Z_2 + Z_{02}\tanh(\gamma L_A)} \end{aligned} \tag{2.18}$$

Using (2.17), we find

$$Z_{L2} = (\frac{Z_L^2}{Z_1}) \frac{Z_L^2/Z_{01} + (Z_L^2/Z_1)\tanh(\gamma L_A)}{Z_L^2/Z_1 + (Z_L^2/Z_{01})\tanh(\gamma L_A)} = \frac{Z_L^2}{Z_{L1}} \tag{2.19}$$

Hence (2.16) holds:

$$\Gamma_{L1} = \frac{Z_{T1} - Z_{L1}}{Z_{T1} + Z_{L1}} = -\Gamma_{L2} = -\frac{Z_{T2} - Z_{L2}}{Z_{T2} + Z_{L2}} \tag{2.20}$$

To take care of propagation in Z_1 and Z_2 we define the reflection coefficients with respect to Z_1 and Z_2 as $\Gamma'_{L1} = (Z_{T1} - Z_1)/(Z_{T1} + Z_1)$ and $\Gamma'_{L2} = (Z_{T2} - Z_2)/(Z_{T2} +$

Z_2). Since

$$Z_{T1} = Z_{L1}\frac{1+\Gamma_{L1}}{1-\Gamma_{L1}}$$
$$Z_{T2} = Z_{L2}\frac{1+\Gamma_{L2}}{1-\Gamma_{L2}} \tag{2.21}$$

we have

$$\Gamma'_{L1} = \frac{\frac{Z_L^2}{Z_{L2}}\frac{1+\Gamma_{L1}}{1-\Gamma_{L1}} - \frac{Z_L^2}{Z_2}}{\frac{Z_L^2}{Z_{L2}}\frac{1+\Gamma_{L1}}{1-\Gamma_{L1}} + \frac{Z_L^2}{Z_2}} = -\Gamma'_{L2} \tag{2.22}$$

Propagation through equal length transmission lines, Z_1 and Z_2 on both sides of Z_L means a rotation of the reflection coefficients, Γ'_{L1} and Γ'_{L2}, in the Smith chart by equal amounts. Hence (2.16) is true.

Consider the two transmission line circuit of Fig. 2.4. In fact, this circuit is a special case of Fig. 2.3 with $L = 0$. So, (2.16) holds for this case as well.

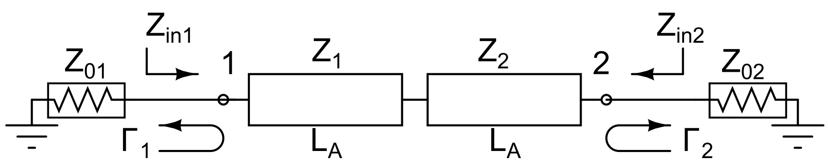

Figure 2.4: Two equal electrical length transmission lines terminated with impedances Z_{01} and Z_{02}. The transmission lines have impedances such that $Z_1Z_2 = Z_{01}Z_{02}$. Z_1 and Z_2 have equal losses.

2.4 Lossy Wilkinson Divider

Fig. 2.5 illustrates a Wilkinson divider. When the divider is excited in the even mode ($a_1 = 0$, $a_2 = a_3 = 1/\sqrt{2}$), using (2.1) the reflected wave from the port 2 can be written as $b_2 = (S_{22} + S_{32})/\sqrt{2}$. So, the reflection coefficient at port 2 for even mode excitation, Γ_{2e}, is given by

$$\Gamma_{2e} = \frac{b_2}{a_2} = S_{22} + S_{32} \tag{2.23}$$

When the divider is excited by a_1=1, $a_2 = a_3 = 0$, we find from (2.1), $b_1 = S_{11}$. For this even mode excitation, the reflection coefficient at port 1, Γ_{1e}, is found as

$$\Gamma_{1e} = \frac{b_1}{a_1} = S_{11} \tag{2.24}$$

The even mode equivalent of the Wilkinson divider reduces to Fig. 2.2 with

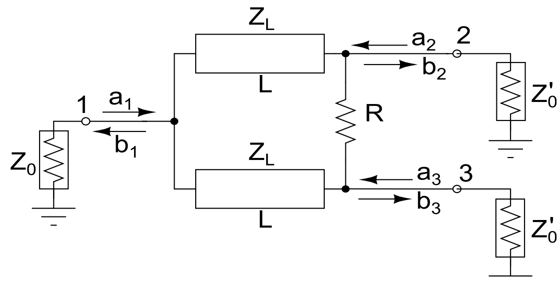

Figure 2.5: A single section Wilkinson divider with a termination of Z_0 at port 1 and Z_0' at ports 2 and 3. $Z_L = \sqrt{2Z_0Z_0'}$

$Z_{01} = 2Z_0$, $Z_{02} = Z_0'$ and $Z_L = \sqrt{2Z_0Z_0'}$. So, (2.16) is valid: $\Gamma_{1e} = -\Gamma_{2e}$. Combining this with (2.23) and (2.24) results in

$$S_{11} + S_{22} + S_{32} = 0 \tag{2.25}$$

(2.25) is a more strict version of (2.6). We note that this equation holds at all frequencies regardless of the value of isolation resistor, R.

2.5 Lossy Multisection Wilkinson Divider

The analysis in the previous part can be generalized to cover the multisection Wilkinson dividers.

Consider the multisection Wilkinson divider shown in Fig. 2.6 with odd number of sections. The transmission lines can be lossy. If the characteristic impedances satisfy the relations

$$Z_L = \sqrt{2Z_0Z_0'} \quad \text{and} \quad Z_1Z_2 = 2Z_0Z_0' \tag{2.26}$$

then the even mode equivalent circuit of the multisection Wilkinson is equivalent to Fig. 2.3 with $Z_{01} = 2Z_0$ and $Z_{02} = Z_0'$. Hence (2.25) is valid.

If the multisection Wilkinson divider has an even number of sections, then we can use the equivalence of Fig. 2.4 with $Z_{01} = 2Z_0$ and $Z_{02} = Z_0'$ and the condition

$$Z_1Z_2 = 2Z_0Z_0' \tag{2.27}$$

Table 2.1: Optimal characteristic impedance values for multisection Wilkinson dividers for Z_0=50Ω [1]

N	1	2	2	3	3	4
Z_3						89.63
Z_1		83.35	81.99	89.89	86.98	77.17
Z_L	70.71			70.71	70.71	
Z_2		59.99	60.98	55.62	54.48	64.79
Z_4						55.79

Therefore, (2.25) is also valid.

Cohn [1] gives the optimum values of impedances for multisection Wilkinson dividers. Table 2.1 lists some of the values given by Cohn. For optimal Wilkinson dividers with odd numbered sections, the conditions of (2.26) are satisfied. On the other hand, for those with even number of sections, (2.27) is satisfied. Therefore, (2.25) is valid for all optimal multisection Wilkinson dividers. The values of isolation resistors, R_1, R_2 and R_3, or the lengths of transmission lines do not play a role for the validity of (2.25).

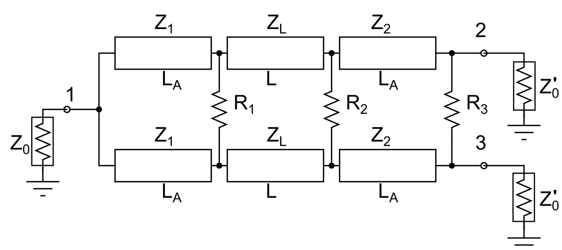

Figure 2.6: A multisection Wilkinson divider with a termination of Z_0 at port 1 and Z_0' at ports 2 and 3.

2.6 Lossy n-Way Wilkinson Divider

Even mode equivalent circuit of a n-way Wilkinson divider is shown in Fig. 2.7. $Z_L = \sqrt{nZ_0Z_0'}$ should be satisfied for optimal power transfer. So, (2.16) is valid. For the n-way Wilkinson circuit, we have $\Gamma_1 = S_{11}$ and $\Gamma_2 = S_{22} + S_{32} + S_{42} +$

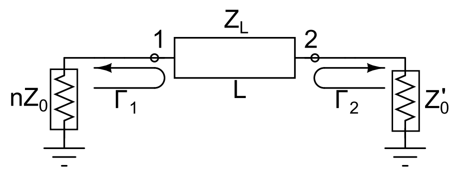

Figure 2.7: Even mode equivalent circuit of the n-way Wilkinson divider with $Z_L = \sqrt{nZ_0 Z_0'}$.

$\ldots + S_{n2}$. Hence we arrive at the result

$$S_{11} + S_{22} + S_{32} + S_{42} + \ldots + S_{n2} = 0 \tag{2.28}$$

Notice that there is no condition for isolation resistors. They may have any arbitrary value (or they may be absent) and they do not have to be all equal.
n-way Wilkinson dividers generally require three dimensional construction for the placement of the isolation resistors. As (2.28) does not depend on the resistor values, it can be verified on planar 2D geometries by avoiding the resistors requiring the third dimension.

2.7 Asymmetric 2-way Wilkinson Divider

Fig. 2.8 shows an asymmetrical Wilkinson power divider. Differing termination resistors and line impedances are used for unequal power division. α^2 and β^2 are power division ratios with $\alpha^2 + \beta^2 = 1$. (2.29) expresses the S-parameter matrix of the divider.

$$\begin{bmatrix} b_1 \\ b_2 \\ b_3 \end{bmatrix} = \begin{bmatrix} S_{11} & S_{21} & S_{31} \\ S_{21} & S_{22} & S_{32} \\ S_{31} & S_{32} & S_{33} \end{bmatrix} \begin{bmatrix} a_1 \\ a_2 \\ a_3 \end{bmatrix} \tag{2.29}$$

where

$$S_{21} = \alpha e^{-j\phi}\sqrt{1 - |S_{11}|^2}\ ,\ S_{31} = \beta e^{-j\phi}\sqrt{1 - |S_{11}|^2} \tag{2.30}$$

For the divider in Fig. 2.8, even mode results when $a_2 = \alpha$ and $a_3 = \beta$ are applied. Using (2.29) it is deduced that $b_2 = \alpha S_{22} + \beta S_{32}$ and $b_3 = \alpha S_{32} + \beta S_{33}$. The equivalent circuit in this excitation scheme is shown in Fig. 2.9-a, midplane is

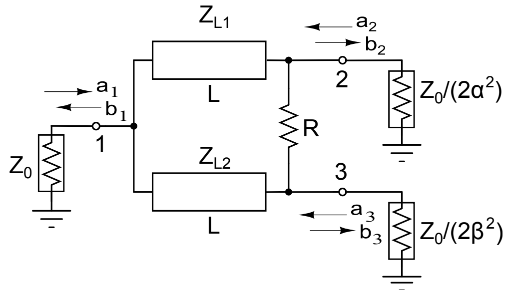

Figure 2.8: An asymmetric Wilkinson divider with $Z_{L1} = Z_0/(\sqrt{2}\alpha^2)$, $Z_{L2} = Z_0/(\sqrt{2}\beta^2)$ and $R = Z_0(1/\alpha^2 + 1/\beta^2)/2$ with $\alpha^2 + \beta^2 = 1$.

open circuited hence the resistor is removed. Port-1 is also decomposed into two parts. The reflection coefficient Γ_2 in Fig. 2.9-a equals b_2/a_2

$$\Gamma_2 = \frac{b_2}{a_2} = \frac{\alpha S_{22} + \beta S_{32}}{\alpha} = S_{22} + \frac{\beta}{\alpha} S_{32} \tag{2.31}$$

Similarly, the reflection coefficient Γ_3 equals b_3/a_3

$$\Gamma_3 = \frac{b_3}{a_3} = \frac{\alpha S_{32} + \beta S_{33}}{\beta} = S_{33} + \frac{\alpha}{\beta} S_{32} \tag{2.32}$$

The upper half and lower half of the circuit in Fig. 2.9-a satisfy the relations expressed in Fig. 2.2 i.e. $\sqrt{(Z_0/\alpha^2)(Z_0/2\alpha^2)} = \sqrt{2} Z_0/2\alpha^2$, $\sqrt{(Z_0/\beta^2)(Z_0/2\beta^2)} = \sqrt{2} Z_0/2\beta^2$. So, (2.16) is valid at both halves of the circuit. So, the reflection coefficients at the left sides equal $-\Gamma_2$ and $-\Gamma_3$ respectively.

When the circuit in Fig. 2.8 is excited from port-1 (a_1=1, $a_2 = a_3 = 0$), the same even mode equivalent circuit shown in Fig.2.9-a is applicable. The reflection coefficient at port-1 (S_{11}) equals to the reflection coefficients at the decomposed ports as explained in Fig.2.9-b. So, $S_{11} = -\Gamma_2 = -\Gamma_3$ in Fig. 2.9-a. Combining this result with (2.31) and (2.32) we find:

$$S_{11} + S_{22} + \frac{\beta}{\alpha} S_{32} = 0 \tag{2.33}$$

$$S_{11} + S_{33} + \frac{\alpha}{\beta} S_{32} = 0 \tag{2.34}$$

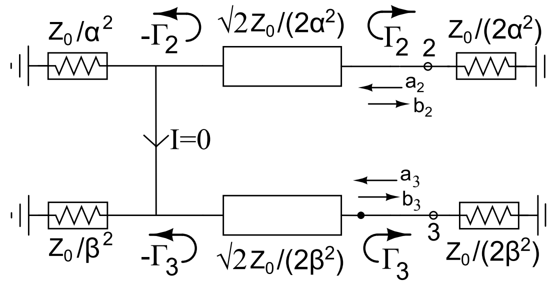

(a)

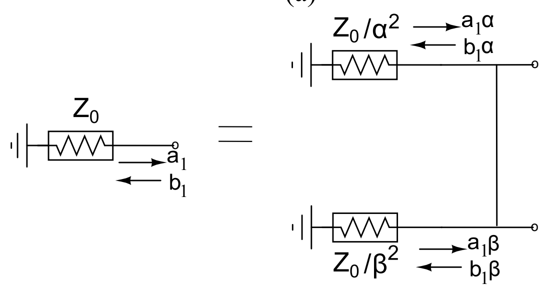

(b)

Figure 2.9: a) Even mode equivalent circuit of the asymmetric Wilkinson divider. b) Port equivalence with $\alpha^2 + \beta^2 = 1$:(Z_0/α^2) in parallel with (Z_0/β^2) results in Z_0. The incident power is a_1^2, in the equivalent representation the incident power is $a_1^2\alpha^2 + a_1^2\beta^2 = a_1^2$, same holds for the reflected power. The node voltage is $(a_1 + b_1)\sqrt{Z_0}$ at all three ports.

2.8 Asymmetric n-way Wilkinson Divider

Fig.2.10-a shows an n-way asymmetric Wilkinson divider. Sum of the power division ratios is equal to one for power conservation, i.e. $\alpha_2^2 + \alpha_3^2 .. + \alpha_{n+1}^2 = 1$. Fig.2.10-b shows the even mode equivalent circuit, Port-1 is decomposed into n parts similar to the two section case. The even-mode can be excited in two schemes. In the first one, we have $a_1 = 1$ and $a_k = 0$ for k=2, k=3,..k=n+1. The other even mode excitation is achieved with $a_1 = 0$ and $a_k = \alpha_k$ for k=2, k=3,..k=n+1.

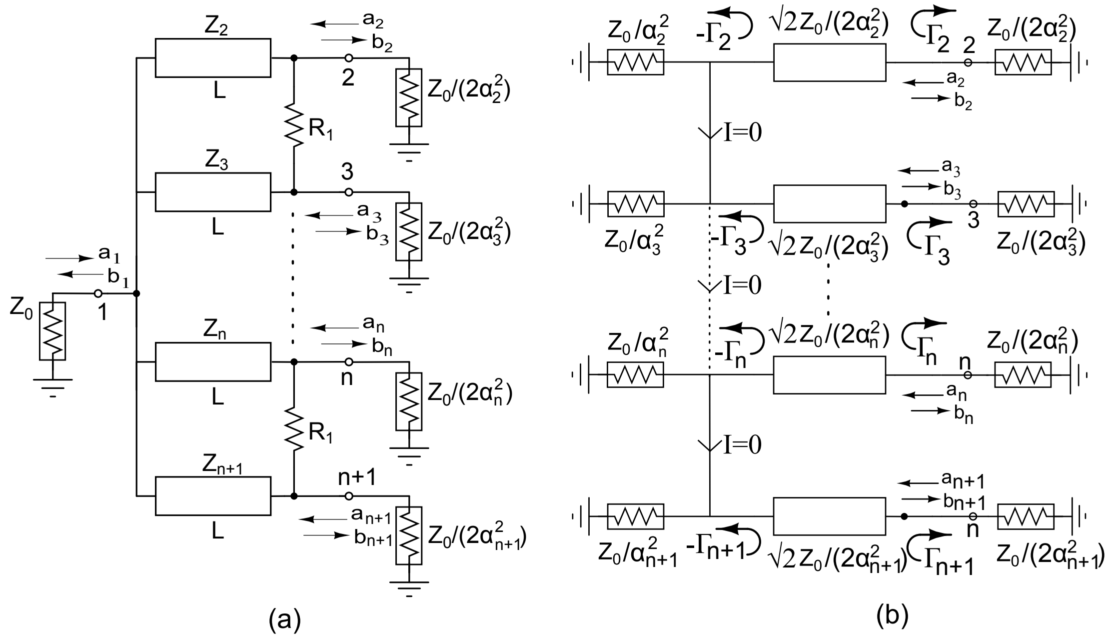

Figure 2.10: a) An asymmetric n-way Wilkinson divider with $Z_2 = Z_0/(\sqrt{2}\alpha_2^2)$, $Z_{n+1} = Z_0/(\sqrt{2}\alpha_{n+1}^2)$ with $\alpha_2^2 + \alpha_3^2 .. + \alpha_{n+1}^2 = 1$. b) Even-mode equivalent circuit of the asymmetric n-way Wilkinson divider

$$\begin{bmatrix} b_1 \\ b_2 \\ b_3 \\ \vdots \\ b_{n+1} \end{bmatrix} = \begin{bmatrix} S_{11} & S_{21} & S_{31} & .. & S_{(n+1)1} \\ S_{21} & S_{22} & S_{32} & .. & S_{(n+1)2} \\ S_{31} & S_{32} & S_{33} & .. & S_{(n+1)3} \\ . & . & . & . & . \\ S_{(n+1)1} & . & . & .. & S_{(n+1)(n+1)} \end{bmatrix} \begin{bmatrix} a_1 \\ a_2 \\ a_3 \\ \vdots \\ a_{n+1} \end{bmatrix} \tag{2.35}$$

(2.35) expresses the S-parameter matrix. In line with the explanations in the previous part, $-\Gamma_2$ in Fig.2.10-b is equal to S_{11}. Γ_2 is the reflection at Port-2 of Fig.2.10-b and it equals to b_2/a_2

$$\Gamma_2 = \frac{b_2}{a_2} = \frac{\alpha_2 S_{22} + \alpha_3 S_{32} + .. + \alpha_{n+1} S_{(n+1)2}}{\alpha_2} \tag{2.36}$$

So, we have

$$S_{11} + S_{22} + \frac{\alpha_3 S_{32} + .. + \alpha_{n+1} S_{(n+1)2}}{\alpha_2} = 0 \tag{2.37}$$

(2.37) can be rewritten as

$$S_{11} + S_{22} + \sum_{i=3}^{n+1} S_{i2}\frac{\alpha_i}{\alpha_2} = 0 \tag{2.38}$$

(2.38) expresses the relation derived using the reflection coefficient at Port-2. We have n S-parameter relations as there are n output ports. (2.39) is valid for k=2, k=3,..,k=n+1.

$$S_{11} + \sum_{i=2}^{n+1} S_{ik}\frac{\alpha_i}{\alpha_k} = 0 \tag{2.39}$$

2.9 The use of equations

The derived relations are summarized in Table-2.2, they are all verified using a microwave circuit simulator. An application of the equation (2.6) is examined in detail in [39]. It was used to design the optimal isolation network for the Wilkinson divider.

The derived equations can be used to reduce the number of optimization goals in an optimization problem, typically encountered in microwave simulators. Consider, for example, an n-way symmetric power divider. It suffices to minimize $|S_{11}|$ and $|S_{22} - (n-1)S_{32}|$. From the relation in (2.11),

$$\begin{aligned} \text{If } |S_{11}| < \delta \;\text{ and }\; |S_{22} - (n-1)S_{32}| < \delta \;\Rightarrow \\ |S_{22}| < \delta \;\text{ and }\; |S_{32}| < \frac{\delta}{n-1} \end{aligned} \tag{2.40}$$

There is no need to have three optimization goals, two are sufficient.

In the 2-way unequal Wilkinson divider, if $\beta/\alpha > 1$, one should try to minimize only $|S_{11}|$ and $|S_{22} - \beta/\alpha\, S_{32}|$, rather than four optimization goals. From (2.33) we have

$$\begin{aligned} \text{If }\; |S_{11}| < \delta \;\text{ and }\; |S_{22} - \frac{\beta}{\alpha}S_{32}| < \delta \;\Rightarrow \\ |S_{22}| < \delta, \quad |S_{32}| < \delta\frac{\alpha}{\beta} \;\text{ and }\; |S_{33}| < \delta\left(1 + \frac{\alpha^2}{\beta^2}\right) \end{aligned} \tag{2.41}$$

Consider a symmetric 3-way Wilkinson divider with asymmetric isolation arms. We have $\alpha_2 = \alpha_3 = \alpha_4$ and hence

$$S_{11} + S_{22} + S_{32} + S_{42} = 0 \tag{2.42}$$

$$S_{11} + S_{33} + 2S_{32} = 0 \tag{2.43}$$

Table 2.2: Summary of the S-parameter Relations

Equation	Valid for
$\lvert S_{11}\rvert = \lvert S_{22} + S_{32}\rvert$ (2.6)	Two way symmetric
$\lvert S_{11}\rvert = \lvert S_{22} + (n-1)S_{32}\rvert$ (2.11)	n-way symmetric
$S_{11} + S_{22} + S_{32} = 0$ (2.25)	Wilkinson
$S_{11} + S_{22} + S_{32} = 0$ (2.25)	Multisection Wilkinson
$S_{11} + S_{22} + (n-1)S_{32} = 0$ (2.28)	n-way Wilkinson
$S_{11} + S_{22} + (\beta/\alpha)S_{32} = 0$ (2.33) $S_{11} + S_{33} + (\alpha/\beta)S_{32} = 0$ (2.34)	Unequal Wilkinson (β^2/α^2: power division ratio)
$S_{11} + \sum_{i=2}^{n+1} S_{ik}\frac{\alpha_i}{\alpha_k} = 0$ for k=2,3,..n+1 (2.39)	n-way unequal Wilkinson

We can combine these equations to get

$$\frac{1}{2}S_{11} + S_{22} - \frac{1}{2}S_{33} + S_{42} = 0 \tag{2.44}$$

From (2.43) and (2.44)

$$\begin{aligned} &\text{If} \quad |S_{11}| < \delta \ \text{ and } \ |S_{33}| < \delta \quad \Rightarrow \\ |S_{32}| < \delta, \quad &\frac{1}{2}|S_{11} + S_{33}| < \delta \ \text{ and } \ |S_{22} + S_{42}| < \delta \end{aligned} \tag{2.45}$$

Moreover

$$\begin{aligned} &\text{If} \quad |S_{22} - S_{42}| < \delta \quad \Rightarrow \\ &|S_{22}| < \delta \ \text{ and } \ |S_{42}| < \delta \end{aligned} \tag{2.46}$$

Therefore we can use just three optimization goals rather than five:

$$\begin{aligned} \text{If} \quad |S_{11}| < \delta, \quad |S_{33}| < \delta \ \text{ and } \ |S_{22} - S_{42}| < \delta \quad \Rightarrow \\ |S_{22}| < \delta, \quad |S_{42}| < \delta \ \text{ and } \ |S_{32}| < \delta \end{aligned} \tag{2.47}$$

Chapter 3

Designing Optimized Isolation Networks for Power Dividers

We aim to design isolation networks that improve the bandwidth of input return loss, output return loss and isolation, simultaneously. This way, the number of sections is not increased hence extra length and loss are avoided. We use the relations derived in the previous chapter relating the input return loss, output return loss and isolation values of a symmetrical two way power divider. Then we calculate the optimal reflection coefficients of the isolation network in the even mode and odd mode cases. Circuits are constructed to realize the calculated reflection coefficients. The resulting circuits are combined in the final divider structure. Detailed analytical work and simulation results for the single and two-section dividers are presented along with new experimental results.

3.1 An S-Parameter Relation

The first S-parameter relation of Chapter-2 is explained again for continuity. In Fig. 3.1, a symmetrical multisection 2-way combiner/divider network is depicted. The network is composed of lossless lumped or distributed components apart from the isolation arms shown with gray boxes. The contents of the gray boxes are delineated in Fig. 3.2. It is composed of symmetrical white boxes with resistors in the middle. The white boxes in Fig. 3.1 and 3.2 can have more than one series or shunt lossless components as long as the symmetry between the arms is maintained. S-parameter matrix equation of such a three port is given by

$$\begin{bmatrix} b_1 \\ b_2 \\ b_3 \end{bmatrix} = \begin{bmatrix} S_{11} & S_{21} & S_{21} \\ S_{21} & S_{22} & S_{32} \\ S_{21} & S_{32} & S_{22} \end{bmatrix} \begin{bmatrix} a_1 \\ a_2 \\ a_3 \end{bmatrix} \tag{3.1}$$

where $|a_n|^2$ and $|b_n|^2$ are the incident and reflected powers at port n. $|S_{21}|$ can be expressed as

$$|S_{21}| = \sqrt{\frac{1 - |S_{11}|^2}{2}} \tag{3.2}$$

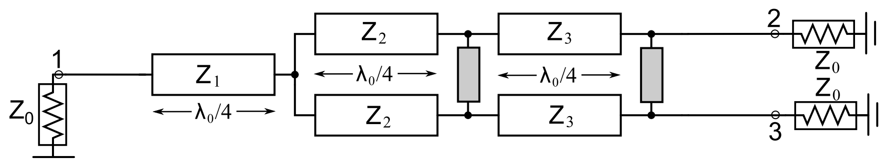

Figure 3.1: A symmetrical 2-way power combiner/divider network. White boxes are lossless. Gray boxes represent the lossy isolation arms.

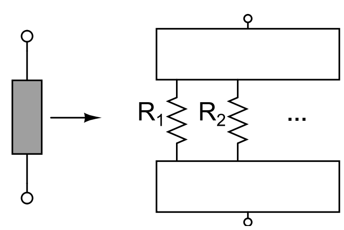

Figure 3.2: Possible contents of a gray box: Symmetrical lossless white boxes with isolation resistors in the middle.

If $a_1 = 0$ and $a_2 = a_3 = 1/\sqrt{2}$ are applied, we find

$$|b_1| = \sqrt{1 - |S_{11}|^2} \tag{3.3}$$

$$b_2 = b_3 = \frac{S_{22} + S_{32}}{\sqrt{2}} \tag{3.4}$$

The incident power is $|a_2|^2 + |a_3|^2 = 1$. Due to the even excitation, there is no dissipation in the isolation arms, and the total incident power equals the transmitted power plus the total reflected power:

$$|a_2|^2 + |a_3|^2 = |b_1|^2 + |b_2|^2 + |b_3|^2 \tag{3.5}$$

From (3.3), (3.4) and (3.5) we find

$$1 = |b_1|^2 + |b_2|^2 + |b_3|^2 = (1 - |S_{11}|^2) + |S_{22} + S_{32}|^2 \tag{3.6}$$

and finally we arrive at the result[1]

$$|S_{11}| = |S_{22} + S_{32}| \tag{3.7}$$

Corollary 1 *For the generic 2-way divider of Fig. 3.1, if* $|S_{22} + S_{32}| < \delta$ *and* $|S_{22} - S_{32}| < \delta$*, then* $|S_{11}| < \delta$*,* $|S_{22}| < \delta$ *and* $|S_{32}| < \delta$*.*

Proof: Defining $S_{22} + S_{32} = \delta_1 e^{j\theta_1}$ and $S_{22} - S_{32} = \delta_2 e^{j\theta_2}$, where $\delta_1, \delta_2 \leq \delta$ and θ_1, θ_2 are arbitrary angles, we have,

$$|S_{22}| = |\delta_1 e^{j\theta_1} + \delta_2 e^{j\theta_2}|/2 \leq (\delta_1 + \delta_2)/2 \leq \delta \tag{3.8}$$

$$|S_{32}| = |\delta_1 e^{j\theta_1} - \delta_2 e^{j\theta_2}|/2 \leq (\delta_1 + \delta_2)/2 \leq \delta \tag{3.9}$$

$|S_{11}| < \delta$ directly follows from (3.7).

For the generalized two-way divider in Fig. 3.1, the excitation $a_1 = 0$, $a_2 = 1$, $a_3 = 1$ results in the even mode operation. The S-parameter matrix equation (3.1) can be rewritten as:

$$\begin{bmatrix} b_1 \\ b_2 \\ b_3 \end{bmatrix} = \begin{bmatrix} S_{11} & S_{21} & S_{21} \\ S_{21} & S_{22} & S_{32} \\ S_{21} & S_{32} & S_{22} \end{bmatrix} \begin{bmatrix} 0 \\ 1 \\ 1 \end{bmatrix} \tag{3.10}$$

So, the reflection coefficient at the second port equals to:

$$\Gamma_e = \frac{b_2}{a_2} = S_{22} + S_{32} \tag{3.11}$$

[1] (3.7) was implicitly stated in [1].

Similarly, the excitation $a_1 = 0$, $a_2 = 1$, $a_3 = -1$ results in the odd mode operation. The S-parameter matrix equation (3.1) can be rewritten as:

$$\begin{bmatrix} b_1 \\ b_2 \\ b_3 \end{bmatrix} = \begin{bmatrix} S_{11} & S_{21} & S_{21} \\ S_{21} & S_{22} & S_{32} \\ S_{21} & S_{32} & S_{22} \end{bmatrix} \begin{bmatrix} 0 \\ 1 \\ -1 \end{bmatrix} \tag{3.12}$$

So, the reflection coefficient at the second port equals to:

$$\Gamma_o = \frac{b_2}{a_2} = S_{22} - S_{32} \tag{3.13}$$

$S_{22} + S_{32}$ and $S_{22} - S_{32}$ are the even mode (Γ_e) and odd mode (Γ_o) reflection coefficients at port 2. From Corollary 1 we can conclude that keeping the even mode and odd mode reflection coefficients at port 2 below a certain level assures that the input-output return loss and isolation parameters are kept below the same level.

In the literature, broadband operation of the power dividers is generally achieved at the expense of an increase in the length and insertion loss of the dividers. In those designs, the isolation networks are composed of floating components without a ground connection, hence the isolation network does not affect the even mode circuit. Consequently, the input return loss can not be tuned by the isolation network. This is a significant loss of a degree of freedom. By the inclusion of components with a ground connection, the isolation network can be active both in the even mode as well as in the odd mode. With such an approach both $S_{22} - S_{32}$ and $S_{22} + S_{32}$ can be tuned by the isolation network.

3.2 An Optimal Choice of Isolation Network in the Even and Odd Modes

Our goal is to find an optimal isolation network for the single-section Wilkinson divider depicted in Fig. 3.3 (a). The isolation network is represented with a gray box. Z_c can be different than $\sqrt{2}Z_0$ for generality. Fig. 3.3 (b) and (c) show the even and odd mode equivalent circuits with the gray box open-circuited and shorted at its mid point, respectively.

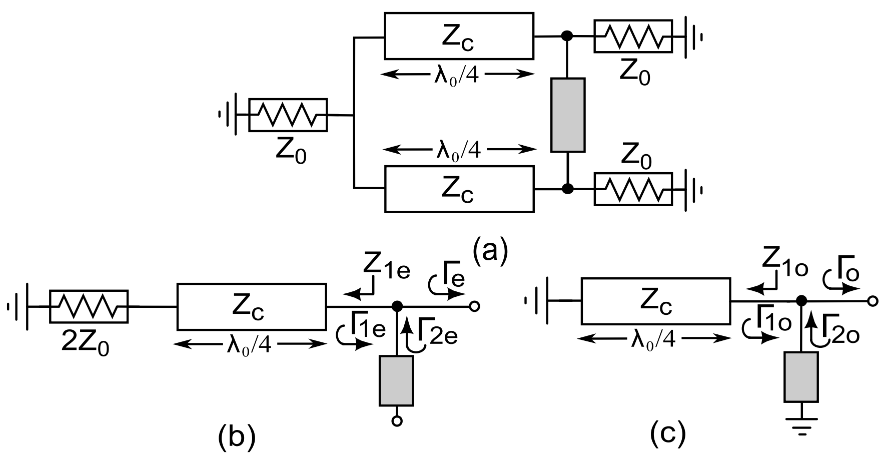

Figure 3.3: a) Single-section Wilkinson divider with a gray box in the isolation arm. b) Even mode equivalent circuit. c) Odd mode equivalent circuit.

For a parallel connection of two one-port networks shown in Fig. 3.4, the perfect match condition (Γ=0) requires:

$$\Gamma_{2m} = \frac{1}{2\overline{Z}_1 - 1} \quad \text{for} \quad \overline{Z}_1 \neq 0 \tag{3.14}$$

where $\overline{Z}_1 = Z_1/Z_0$ is the normalized input impedance of the first block and Γ_{2m} is the input reflection coefficient of the second block giving the perfect match.

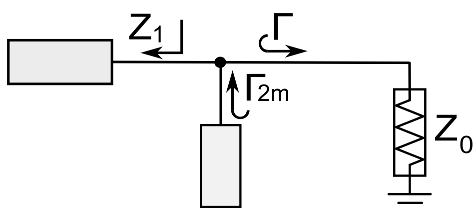

Figure 3.4: Two networks connected in parallel. One has an input impedance of Z_1, the other one has an input reflection coefficient of Γ_{2m} to give Γ=0.

The normalized impedances $\overline{Z}_{1e}$ and $\overline{Z}_{1o}$ defined in Fig. 3.3 are equal to:

$$\overline{Z}_{1e} = \frac{Z_{1e}}{Z_0} = \frac{2 + j\overline{Z}_c \tan(\frac{\pi f}{2f_0})}{1 + j\frac{2}{\overline{Z}_c}\tan(\frac{\pi f}{2f_0})} \tag{3.15}$$

$$\overline{Z}_{1o} = \frac{Z_{1o}}{Z_0} = j\overline{Z}_c \tan(\frac{\pi f}{2f_0}) \tag{3.16}$$

where f_0 ($=w_0/2\pi$) is the center frequency and $\overline{Z}_c$=Z_c/Z_0. The reflection coefficients Γ_{2em} and Γ_{2om} of the even and odd mode isolation circuits that will generate a perfect match can be calculated using (3.14), (3.15) and (3.16):

$$\Gamma_{2em} = \frac{1 + j\frac{2}{\overline{Z}_c}\tan(\frac{\pi f}{2f_0})}{3 + j(2\overline{Z}_c - \frac{2}{\overline{Z}_c})\tan(\frac{\pi f}{2f_0})} \tag{3.17}$$

$$\Gamma_{2om} = \frac{1}{j2\overline{Z}_c\tan(\frac{\pi f}{2f_0}) - 1} \tag{3.18}$$

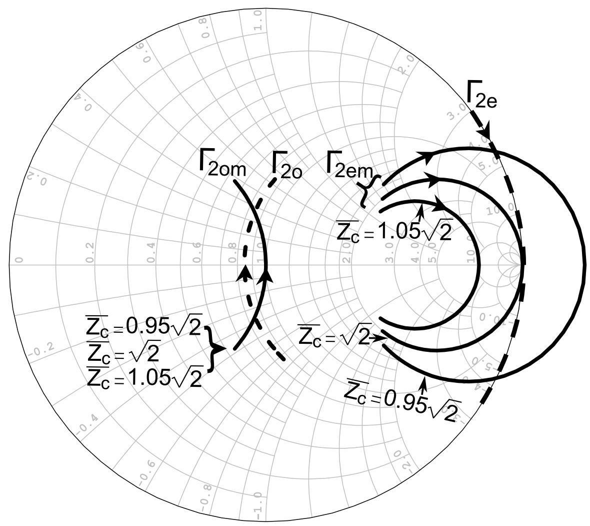

Figure 3.5: Γ_{2em} and Γ_{2om} on the Smith chart (solid lines) as the frequency is swept from $f_0/2$ to $3f_0/2$ (in the direction of arrows) for $\overline{Z}_c$=$0.95\sqrt{2}$, $\sqrt{2}$ and $1.05\sqrt{2}$. Approximations, Γ_{2e} and Γ_{2o}, (dashed lines) are also shown. The trace out of the unitary circle of the Smith Chart might be confusing at first glance. It plots the required reflection coefficients for perfect matching. Consider the matching of 25Ω impedance to the 50Ω system impedance using a shunt component. So you need a −50Ω resistance implying a reflection coefficient out of the unitary circle of the Smith Chart.

3.2.1 Even Mode Isolation Circuit

The trajectory of Γ_{2em} is drawn on the Smith chart of Fig. 3.5 for $\overline{Z}_c$=$0.95\sqrt{2}$, $\sqrt{2}$ and $1.05\sqrt{2}$. Even mode isolation circuit must be lossless, otherwise the insertion loss of the divider will increase. So, its reflection coefficient must lie on the unity circle of the Smith chart. Γ_{2em} characteristic can be approximated with a shorted quarter-wave stub of impedance Z_p as in Fig. 3.6. The corresponding Γ_{2e} is depicted by dashed lines in Fig. 3.5. For $\overline{Z}_c = \sqrt{2}$, Γ_{2e} and Γ_{2em} coincide only at the center frequency and deviate fast with frequency. For $\overline{Z}_c > \sqrt{2}$, the situation is even worse. With $\overline{Z}_c < \sqrt{2}$, Γ_{2e} and Γ_{2em} coincide at two frequencies and the highest deviation occurs at the center frequency, f_0, and at band edges. This characteristic resembles a second degree Chebyshev response maximizing the bandwidth. So, we choose $\overline{Z}_c < \sqrt{2}$ to have a wide-band approximation. The deviation at f_0 can be adjusted by the value of Z_c. At f_0, the shorted quarter-wave stub (Z_p) acts like an open-circuit. Using Corollary-1 we aim to satisfy $|\Gamma_e| \leq \delta$. The deviation is maximum at f_0, so $|\Gamma_e(f_0)| = \delta$. Referring to Fig. 3.6, since $\Gamma_e = \Gamma_{1e}$ at f_0, the value of $Z_{1e}(f_0)$ is equal to

$$Z_{1e}(f_0) = \frac{Z_c^2}{2Z_0} = Z_0\frac{1-\delta}{1+\delta} \tag{3.19}$$

Hence we have

$$\overline{Z}_c = \sqrt{\frac{2(1-\delta)}{1+\delta}} \approx \sqrt{2}(1-\delta) \tag{3.20}$$

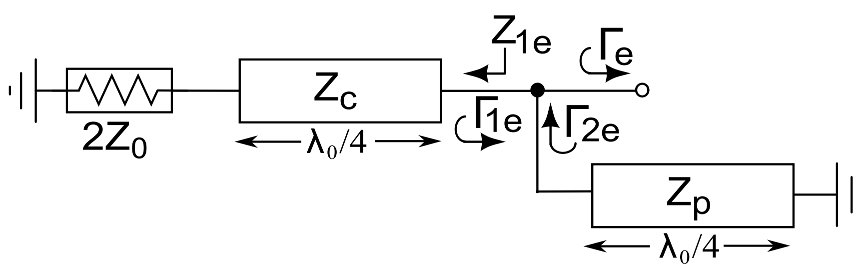

Figure 3.6: Even mode equivalent circuit with the shorted quarter-wave stub of impedance Z_p at the isolation arm.

To calculate the bandwidth and the optimal value of Z_p, we refer to the Smith chart shown in Fig. 3.7. The goal is to bend the Z_{1e} trajectory into the $|\Gamma_e| = \delta$ circle using the shorted transmission line with the characteristic impedance of Z_p. The lowest normalized conductance on the locus of the $|\Gamma_e| = \delta$ circle is $(1-\delta)/(1+\delta)$. So, the frequencies at which Z_{1e} results a conductance of

$(1-\delta)/(1+\delta)$ are the minimum and the maximum frequencies satisfying the $|\Gamma_e| \leq \delta$ condition. The lower and upper frequencies are marked as f_1 and f_2, respectively, in Fig.3.7.

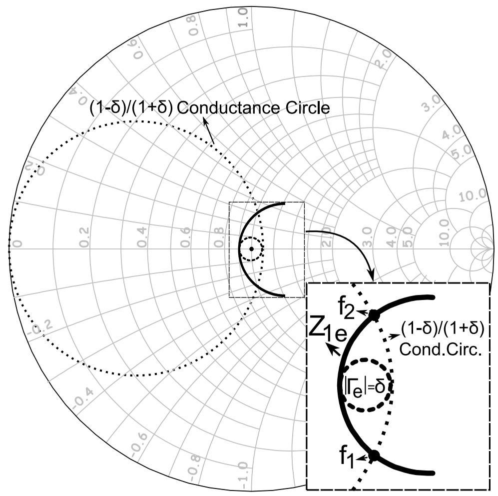

Figure 3.7: Trajectories of the $(1-\delta)/(1+\delta)$ constant conductance circle and $|\Gamma_e| = \delta$ circle along with the trajectory of Z_{1e} (shown in Fig. 3.6).

At f=f_1, we have:

$$\mathcal{Re}\left\{\frac{1}{\overline{Z}_{1e}(f_1)}\right\} = \frac{1-\delta}{1+\delta} \tag{3.21}$$

Using (3.15) and (3.20), (3.21) can be expanded as:

$$\mathcal{Re}\left\{\frac{\sqrt{2}(1-\delta) + j2\tan(\frac{\pi f_1}{2f_0})}{2(1-\delta)[\sqrt{2} + j(1-\delta)\tan(\frac{\pi f_1}{2f_0})]}\right\} = \frac{1-\delta}{1+\delta} \tag{3.22}$$

We find

$$\tan(\frac{\pi f_1}{2f_0}) = \sqrt{\frac{1-3\delta}{4\delta - 3\delta^2 + \delta^3}} \tag{3.23}$$

For small δ, we can ignore the δ^3 term, and write f_1 as:

$$\frac{f_1}{f_0} \approx \frac{2}{\pi}\tan^{-1}\sqrt{\frac{1-3\delta}{4\delta - 3\delta^2}} \tag{3.24}$$

We note that $f_2 - f_0 = f_0 - f_1$. For example, for δ=0.1 (-20 dB), f_1=$0.6f_0$ and f_2=$1.4f_0$.

The value of Z_p is calculated by considering that the imaginary part of the $1/Z_{1e}$ admittance should be compensated perfectly at f_1:

$$Im\left\{\frac{1}{\overline{Z}_{1e}}\right\} = \frac{1}{\overline{Z}_p \tan(\frac{\pi f_1}{2f_0})} \tag{3.25}$$

So, we have

$$Im\left\{\frac{\sqrt{2}(1-\delta) + j2\tan(\frac{\pi f_1}{2f_0})}{2(1-\delta)[\sqrt{2} + j(1-\delta)\tan(\frac{\pi f_1}{2f_0})]}\right\} = \frac{1}{\overline{Z}_p \tan(\frac{\pi f_1}{2f_0})} \tag{3.26}$$

Using (3.24) the value of $\overline{Z}_p$ is extracted from (3.26) as:

$$\overline{Z}_p \approx \sqrt{2}\frac{1+2\delta-2\delta^2}{1-\delta-7\delta^2} \tag{3.27}$$

$\overline{Z}_p$ approaches to $\sqrt{2}$ as δ gets closer to zero. With δ=0.1, (3.27) results in $\overline{Z}_p$=2.0.

If a lumped circuit is preferred, this shorted $\lambda/4$ line can be approximated as a parallel LC circuit [40] with the component values expressed as:

$$w_0 L_p = \frac{4Z_p}{\pi} \text{ and } L_p C_p = \frac{1}{w_0^2} \tag{3.28}$$

3.2.2 Odd Mode Isolation Circuit

Smith chart trajectories of Γ_{2om} for three different Z_c values (which are almost equal to each other) are shown in Fig. 3.5. The locus of Γ_{2om} follows a constant conductance circle. A series RLC circuit resonant at f_0 shown in Fig. 3.8 can be utilized to approximate the desired characteristics.

The same approach as the even mode case is followed to calculate the component values of the odd mode isolation network analytically. Referring to Fig. 3.8, Γ_{2o} is the reflection coefficient of the series $R_oL_oC_o$ network. The goal is to maximize the bandwidth of the $|\Gamma_o| \leq \delta$ condition. Fig. 3.9 shows the $|\Gamma| = \delta$ circle on the Smith chart together with the trajectory of Γ_{2o}. The points marked as f_3 and f_4 represent the edge frequencies that Γ_{2o} can be fitted into the $\Gamma = \delta$ circle by the shorted stub of impedance Z_c.

The impedance of a series LC resonator is not symmetric around the center frequency. We have $f_4 - f_0 > f_0 - f_3$. Therefore, $2(f_0 - f_3)$ is the bandwidth

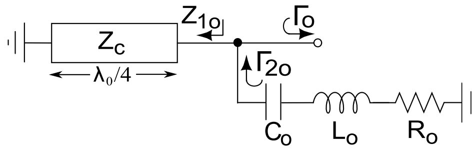

Figure 3.8: Odd mode equivalent circuit with the optimal isolation network. L_o and C_o are resonant at the center frequency f_0.

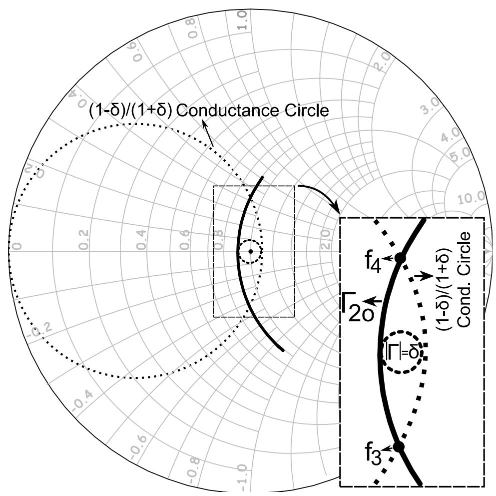

Figure 3.9: Trajectories of the $(1-\delta)/(1+\delta)$ constant conductance circle and $|\Gamma| = \delta$ circle along with the trajectory of Γ_{2o} of Fig. 3.8.

of the $|\Gamma_o| \leq \delta$ condition. For the circuit in Fig. 3.8 at f_0, C_o resonates with L_o and the quarter-wave stub Z_c is open-circuit. We have $\Gamma_o(f_0) = \Gamma_{2o}(f_0) = (R_o - Z_0)/(R_o + Z_0)$. As shown in Fig. 3.9, $\Gamma_{2o}(f_0) = -\delta$. So, the value of the resistor is equal to:

$$\overline{R}_o = \frac{R_o}{Z_0} = \frac{1-\delta}{1+\delta} \tag{3.29}$$

L_o can be calculated by imposing two conditions at $f = f_3$. Γ_{2o} trajectory crosses the $(1-\delta)/(1+\delta)$ conductance circle and the transmission line with the impedance of Z_c compensates the reactive part of Γ_{2o} perfectly. So, we have two equations:

$$\mathcal{Re}\left\{\frac{Z_0}{R_o - j2\pi f_3 L_o\left(\frac{f_0^2}{f_3^2} - 1\right)}\right\} = \frac{1-\delta}{1+\delta} \tag{3.30}$$

$$Im\left\{\frac{Z_0}{R_o - j2\pi f_3 L_o\left(\frac{f_0^2}{f_3^2}-1\right)}\right\} = \frac{1}{\overline{Z}_c \tan(\frac{\pi f_3}{2f_0})} \tag{3.31}$$

Using (3.29) and (3.30) we find:

$$2\pi f_3 \frac{L_o}{Z_0}\left(\frac{f_0^2}{f_3^2}-1\right) = \frac{2\sqrt{\delta}}{1+\delta} \tag{3.32}$$

Inserting (3.32) in the denominator of (3.31) and using (3.20), f_3 is calculated as:

$$\frac{f_3}{f_0} = \frac{2}{\pi}\tan^{-1}\left(\frac{(1+\delta)^{3/2}}{\sqrt{8\delta(1-\delta)}}\right) \tag{3.33}$$

(3.33) together with (3.32) result in:

$$\frac{w_0 L_o}{Z_0} = \frac{2\sqrt{\delta}}{1+\delta}\frac{\frac{f_0}{f_3}}{\left(\frac{f_0}{f_3}\right)^2 - 1} \tag{3.34}$$

For example, with Z_0=50Ω and δ=0.1, we find f_3=0.596f_0 and L_o=4.23nH. We note that the odd mode bandwidth is greater than the even mode bandwidth.

3.3 Combining the Even And Odd Mode Isolation Networks

We merge the isolation circuits of Fig. 3.6 and Fig. 3.8 as shown in Fig. 3.10. Fig. 3.11 depicts the approximations involved in the merging process. Due to the interaction between the even and odd mode networks, some component values are shown with a prime symbol to indicate a possible modification in the calculated component values of the previous section.

The value of Z_c was determined in the even mode circuit by the condition at f_0. Since the isolation network does not affect the even mode circuit at f_0, Z_c value of (3.20) will not be modified. Similarly, R_o was determined in the odd mode circuit by the condition at f_0. Since Z_p' is open circuit at f_0, the value of R_0 given in (3.29) will not change.

The new values of Z_p' and L_0' can be calculated following the analysis of the previous sections. Fig. 3.12 shows the even and odd mode equivalent circuits of

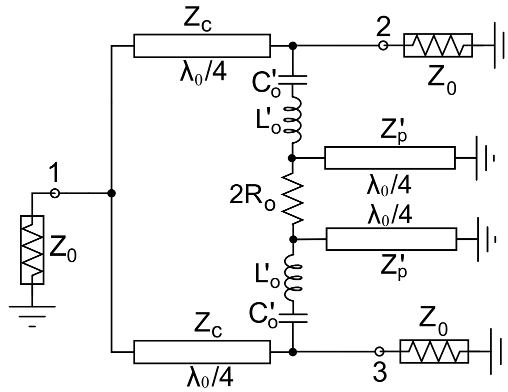

Figure 3.10: Schematic diagram of the divider by merging the optimal even mode and odd mode isolation networks.

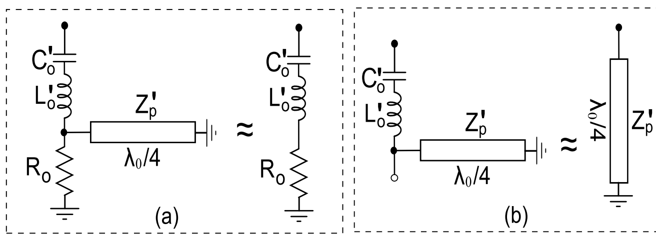

Figure 3.11: Equivalent representation of the isolation network for the divider in Fig. 3.10. a) Odd-mode b) Even-mode

the divider. Referring to Fig. 3.12(a), (3.26) is modified due to the presence of L'_o and C'_o:

$$\mathit{Im}\left\{\frac{\sqrt{2}(1-\delta)+j2\tan(\frac{\pi f_1}{2f_0})}{2(1-\delta)[\sqrt{2}+j(1-\delta)\tan(\frac{\pi f_1}{2f_0})]}\right\} = = \frac{Z_0}{Z'_p\tan(\frac{\pi f_1}{2f_0})-2\pi f_1 L'_o\left(\frac{f_0^2}{f_1^2}-1\right)} \tag{3.35}$$

where f_1 is expressed in (3.24). f_1 is independent of the problem handled here, it is determined solely by Z_c.

From Fig. 3.12(b), (3.30) and (3.31) are modified to

$$\mathcal{Re}\left\{\frac{Z_0}{R_o \parallel jZ'_p\tan(\frac{\pi f'_3}{2f_0})-j2\pi f'_3 L'_o\left(\frac{f_0^2}{f_3'^2}-1\right)}\right\} = \frac{1-\delta}{1+\delta} \tag{3.36}$$

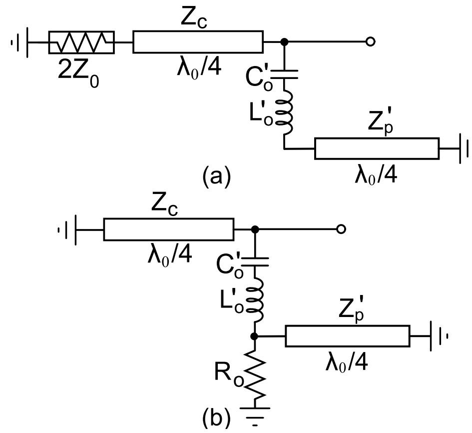

Figure 3.12: Even (upper) and odd (lower) mode equivalent circuits of the divider in Fig. 3.10

$$Im\left\{\frac{Z_0}{R_o \parallel jZ'_p \tan(\frac{\pi f'_3}{2f_0}) - j2\pi f'_3 L'_o\left(\frac{f_0^2}{f_3'^2}-1\right)}\right\} = \\ = \frac{Z_0}{Z_c \tan(\frac{\pi f'_3}{2f_0})} \tag{3.37}$$

f'_3 is used instead of the f_3 in (3.33) because it is dependent on Z'_p and L'_o. A simultaneous solution of (3.35), (3.36) and (3.37) to find f'_3, Z'_p and L'_o is not possible. To find the values, the mean square error in these equations are minimized numerically. Results of the numerical calculations are used to express Z'_p and L'_o by the following approximations

$$\overline{Z}'_p = \frac{Z'_p}{Z_0} \approx \sqrt{2} + 10\delta \tag{3.38}$$

$$\overline{w_0 L}'_o = \frac{w_0 L'_o}{Z_0} \approx 1.1 - 4.6\delta \tag{3.39}$$

Table 3.1 lists the results normalized with Z_0. The achievable normalized bandwidth and required component values for the corresponding δ level are listed. The divider bandwidth, Δf, is limited by the bandwidth of the even mode circuit: Δf=$2(f_0 - f_1)$. Z_c, f_1, R_o, Z'_p and L'_o are determined from (3.20), (3.24), (3.29), (3.38) and (3.39), respectively. C'_o is resonant with L'_o at f_0. Our results are verified using a microwave circuit simulator[2].

[2]AWR Corp. El Segundo, CA 90245, USA, http://www.awrcorp.com

Table 3.1: Normalized component values for input-output return losses and isolation better than δ (dB).

δ (dB)	$\Delta f/f_0$	$\overline{Z}_c$	$2\overline{R}_o$	$\overline{w_0 L_o'}$	$\overline{Z}_p'$
-20	0.80	1.28	1.63	0.64	2.41
-25	0.60	1.34	1.79	0.84	1.98
-30	0.45	1.37	1.88	0.96	1.73
-35	0.34	1.39	1.93	1.02	1.59
-40	0.25	1.4	1.96	1.06	1.51

It is possible to apply the proposed method to a two-section divider. Using a similar isolation arm for both sections, it is possible to extend the bandwidth considerably. The results for the two-section case are given in the last section of this chapter.

Fig. 3.13 compares the bandwidth capabilities of the proposed single-section and two-section dividers with the classical single-section Wilkinson divider and Cohn's two-section Wilkinson divider [1]. A significant bandwidth improvement is achieved. For 25 dB of input-output return loss and isolation, three times wider bandwidth is obtained in comparison to a single-section Wilkinson. The bandwidth of a two-section Wilkinson divider is almost reached with a single-section divider, avoiding the extra size and insertion loss of the two-section divider.

In terms of insertion loss, the proposed divider is similar to a single-section Wilkinson divider, because the input signal propagates a distance of exactly one quarter wavelength. In fact, our divider is more advantageous in terms of the loss, since the impedance transforming line has a characteristic impedance smaller than $\sqrt{2}Z_0$ resulting in a wider line width. Considering the size of the divider, the $\lambda_0/4$ line in the isolation arm is shorted at one end and it has a high characteristic impedance with a narrow width. This enables one to use layout techniques such as bending or meandering of the line to get a compact size. We note that a two-section Wilkinson divider with two isolation resistors cannot be shaped in the same manner to reduce the size.

We note that presence of a ground path in the isolation network generates nulls in S_{21}. These frequencies can be calculated by considering the sum of the

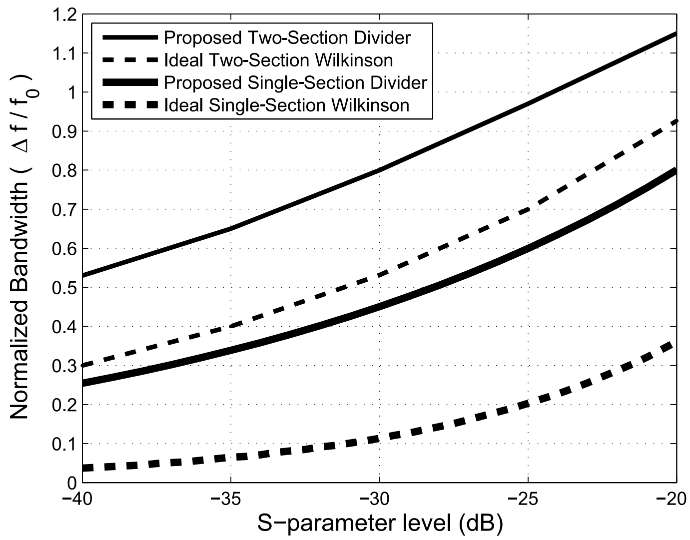

Figure 3.13: Normalized bandwidth comparison of the prosed divider structure with the classical single-section Wilkinson divider and Cohn's design of two- section Wilkinson divider [1].

impedances of the Z'_p line and $L'_oC'_o$ pair:

$$Z'_p \tan(\frac{\pi f}{2f_0}) - 2\pi f L'_o \left(\frac{f_0^2}{f^2} - 1\right) = 0 \tag{3.40}$$

Using (3.38) and (3.39), (3.40) can be rewritten as

$$(\sqrt{2} + 10\delta) \tan(\frac{\pi f}{2f_0}) = (1.1 - 4.6\delta)\frac{f}{f_0}\left(\frac{f_0^2}{f^2} - 1\right) \tag{3.41}$$

For example, for $\delta = 0.1$ (-20 dB), (3.41) is satisfied at two frequencies, at $0.36f_0$ and $1.8f_0$, outside the operation bandwidth ($0.6f_0$-$1.4f_0$) of the divider.

3.4 Simulation and Experimental Results

The proposed divider in Fig. 3.10 is implemented for experimental verification at a center frequency of f_0=1 GHz. δ=-20 dB is the design goal. As shown in Table 3.1, the theoretical fractional bandwidth is $\Delta f/f_0$=0.8 implying a 20 dB bandwidth of 0.6 GHz to 1.4 GHz. The divider is simulated using the microwave circuit simulator and an electromagnetic simulator[3]. With ideal components, $\Delta f/f_0 = 0.8$ is achieved using the values given in Table 3.1. Inclusion of the junction effects and component parasitics result in a reduction of the bandwidth. To alleviate these effects, the component values are tuned slightly.

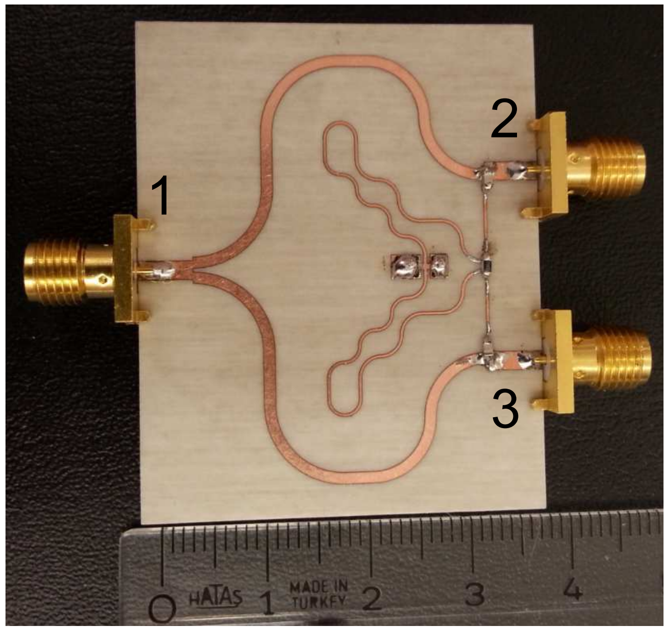

Figure 3.14: Implemented 2-way power divider of Fig. 3.10.

Fig. 3.14 shows the photo of the divider implemented on a RO4003[4] substrate with a thickness of 0.8 mm. L_o inductors are implemented using high impedance microstrip lines of 0.3 mm in width and 6.7 mm in length. Presence of L_o in the isolation circuit provides a natural separation between ports 2 and 3, reducing the length of subsequent connections and improving the isolation between the output ports [41],[42]. In the divider of Fig. 3.14, the width of Z_c lines are 1.1 mm corresponding to a characteristic impedance of 66 Ω. Z_p lines have a width of 0.3 mm resulting in an impedance of 116 Ω. 0603 package 5.6 pF capacitors and a 75 Ω resistor are used. Fig. 3.15 and 3.17 show the simulation results of the electromagnetic simulator. The output return loss and the isolation are better than 20 dB in the targeted bandwidth, the input return loss drops to 17 dB at

[3]SONNET Software, North Syracuse NY 13212, USA, http://www.sonnetsoftware.com

[4]Rogers Corp. Rogers, CT 06263, USA, http://www.rogerscorp.com

the band edges due to the nonideal effects.

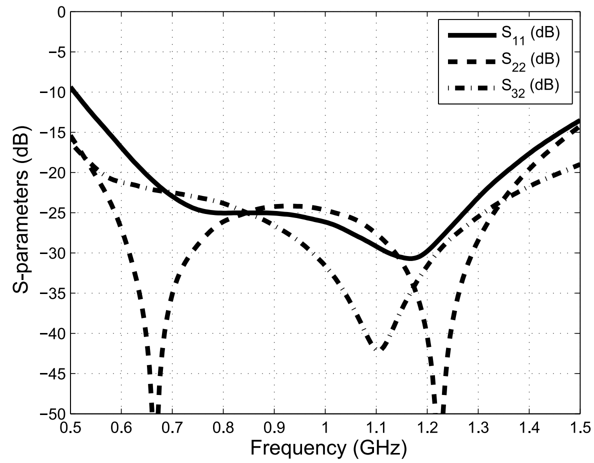

Figure 3.15: Simulated S-parameter characteristics of the divider in Fig. 3.14.

Measured input-output return loss, isolation and insertion loss responses are shown in Fig. 3.16 and 3.17. The measurement results match the simulation results well. In the operation band, the extra insertion loss is less than 0.2 dB and the amplitude mismatch between the output ports is lower than 0.025 dB.
As discussed in (3.28) of Section 3.2.1, the shorted $\lambda_0/4$ lines at the isolation arm can be replaced with lumped components. For a verification, a modified version of the divider in Fig. 3.14 is implemented (Fig. 3.18). (3.28) results in L_p=23.5 nH and C_p=1.08 pF for 116 Ω characteristic impedance and 1 GHz center frequency. Available chip inductor with a value closest to the calculated one is a 20 nH 0805 package chip inductor. S-parameter data provided by the manufacturer shows that the equivalent inductance of the 20 nH chip inductor increases up to 35 nH at 2 GHz due to the parasitic capacitance. This requires a reduction in the calculated value of C_p. The best performance is obtained using a 0.8 pF capacitor. Fig. 3.19 and Fig. 3.20 show the simulated and measured results, respectively. The characteristic is similar to the case with the shorted line. 19 dB bandwidth spans the 0.6 GHz to 1.35 GHz frequency range. The insertion loss is again below 0.2 dB in the operation bandwidth.

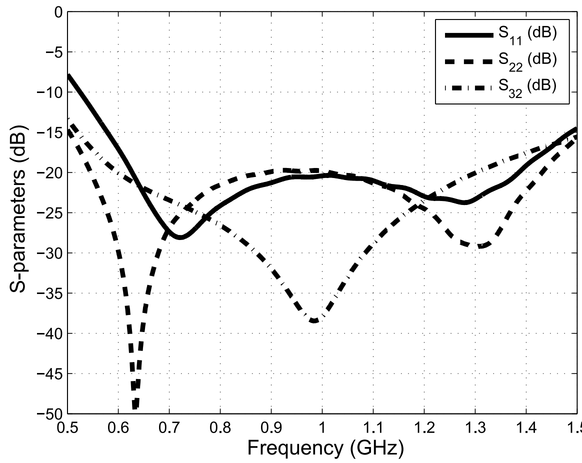

Figure 3.16: Measured S-parameter characteristics of the divider in Fig. 3.14.

Table 3.2 is a comparison[5] of the dividers of recent studies. Given normalized bandwidth values are valid at the specified dB values of input return loss, output return loss and isolation. Our designs have a wide bandwidth with a low insertion loss and compact size, at the expense of the increased number of components. This increases the circuit implementation complexity and the parasitic problem.

3.5 Two-Section Divider With the Optimized Isolation Networks

The optimized isolation network is applied to the two-section case as shown in Fig. 3.21. The even mode and odd mode equivalent circuits are shown in Fig. 3.22. Z_{ine} and Z_{ino} represent the input impedances in each mode respectively.
At f_0, the even mode circuit shown in Fig. 3.22 (a) is composed of only Z_{c1} and Z_{c2}. They provide an impedance transformation from $2Z_0$ to Z_0. The optimal impedance values satisfy the geometric mean condition [47]:

$$Z_{c1}Z_{c2} = 2Z_0^2 \tag{3.42}$$

[5]The loss comparison in the table is not totally fair, because the upper frequencies and the substrate materials of the dividers listed in the table are not the same.

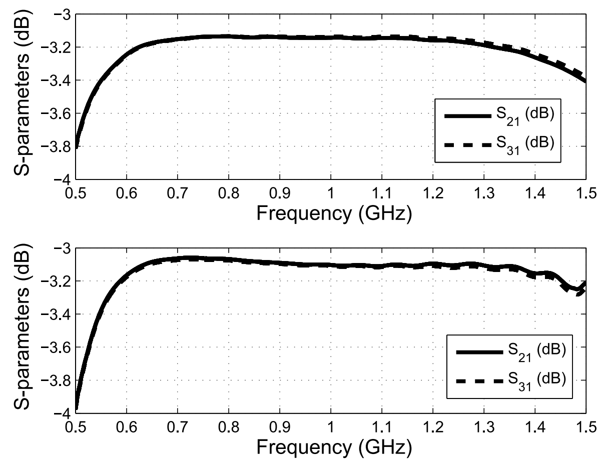

Figure 3.17: Simulated (upper) and measured (lower) S-parameter characteristics of the divider in Fig. 3.14.

By allowing a nonzero reflection coefficient magnitude of δ, the bandwidth of operation can be extended. At the band center, f_0, we have a real reflection coefficient of δ [48]. So, we can write

$$\frac{Z_{c2}^2\, 2Z_0}{Z_{c1}^2} = Z_0 \frac{1+\delta}{1-\delta} \tag{3.43}$$

Using (3.42) and (3.43), Z_{c1} and Z_{c2} are calculated as:

$$\overline{Z}_{c1} = \frac{Z_{c1}}{Z_0} \approx 2^{3/4}(1-\delta/2) \tag{3.44}$$

$$\overline{Z}_{c2} = \frac{Z_{c2}}{Z_0} \approx 2^{1/4}(1+\delta/2) \tag{3.45}$$

Even mode input impedance can be expressed as:

$$Z_{ine} = \left(Z_{c2} \frac{Z_x + jZ_{c2}\tan(\frac{\pi f}{2f_0})}{Z_{c2} + jZ_x \tan(\frac{\pi f}{2f_0})} \right) \parallel \left(j2\pi f L_2 (1 - \frac{f_0^2}{f^2}) + \frac{j2\pi f L_4}{1 - \frac{f_0^2}{f^2}} \right) \tag{3.46}$$

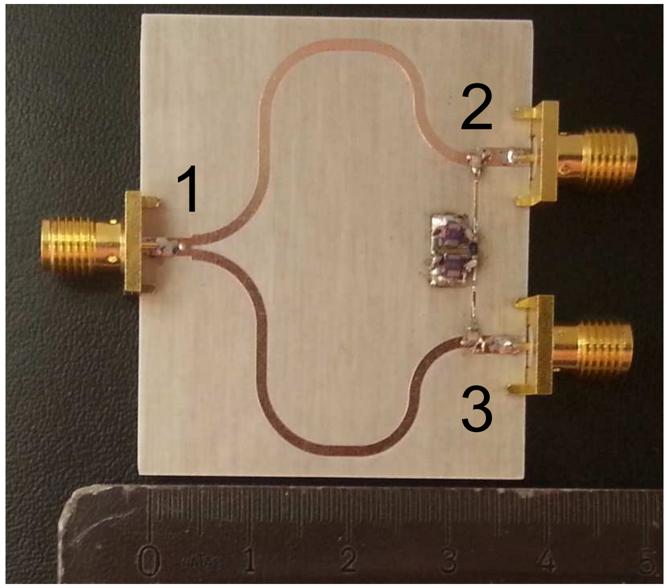

Figure 3.18: Modified version of divider in Fig. 3.14 upon the replacement of the shorted $\lambda_0/4$ lines with the parallel LC resonators.

where

$$Z_x = \left(Z_{c1} \frac{2Z_0 + jZ_{c1}\tan(\frac{\pi f}{2f_0})}{Z_{c1} + j2Z_0\tan(\frac{\pi f}{2f_0})} \right) \parallel \left(j2\pi f L_1 (1 - \frac{f_0^2}{f^2}) + \frac{j2\pi f L_3}{1 - \frac{f_0^2}{f^2}} \right) \quad (3.47)$$

The odd mode input impedance can be expressed as:

$$Z_{ino} = \left(Z_{c2} \frac{Z_y + jZ_{c2}\tan(\frac{\pi f}{2f_0})}{Z_{c2} + jZ_y\tan(\frac{\pi f}{2f_0})} \right) \parallel \left(j2\pi f L_2 (1 - \frac{f_0^2}{f^2}) + \left(\frac{j2\pi f L_4}{1 - \frac{f_0^2}{f^2}} \parallel R_2 \right) \right) \quad (3.48)$$

where

$$Z_y = jZ_{c1}\tan(\frac{\pi f}{2f_0}) \parallel \left(j2\pi f L_1 (1 - \frac{f_0^2}{f^2}) + \left(\frac{j2\pi f L_3}{1 - \frac{f_0^2}{f^2}} \parallel R_1 \right) \right) \quad (3.49)$$

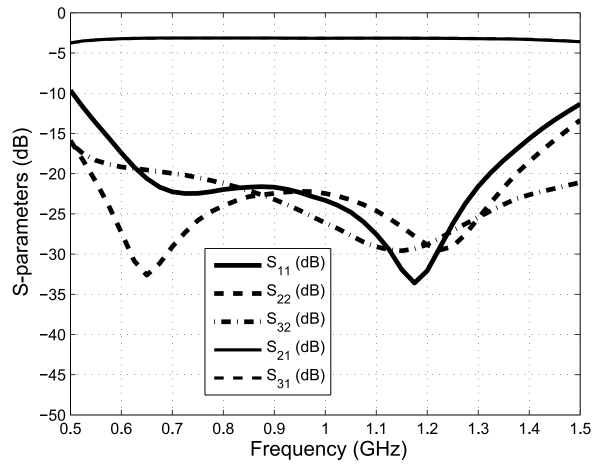

Figure 3.19: Simulated response of the divider in Fig. 3.18.

The optimal values of the remaining components are found by solving (3.46) and (3.48) numerically for the maximal bandwidth. The results indicate that the L_1, C_1 pair is not needed. For 20 dB and 25 dB cases L_3, C_3 pair is also absent and hence the first isolation network consists of only a resistor, $2R_1$. The normalized component values verified using a microwave circuit simulator are tabulated in Table 3.3. The performance of this divider is depicted in Fig. 3.13. Its bandwidth is considerably better than that of a two-section Wilkinson divider.

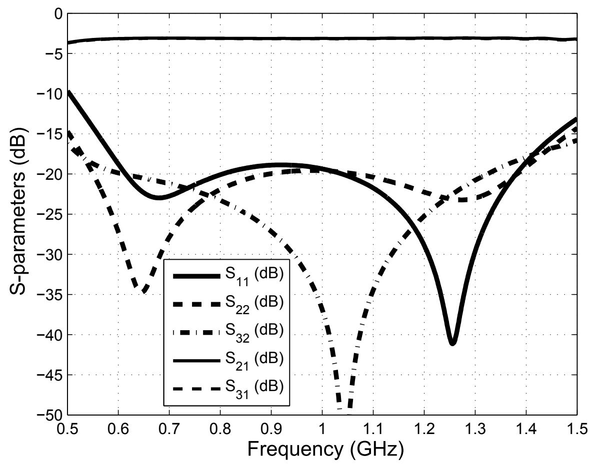

Figure 3.20: Measured response of the divider in Fig. 3.18.

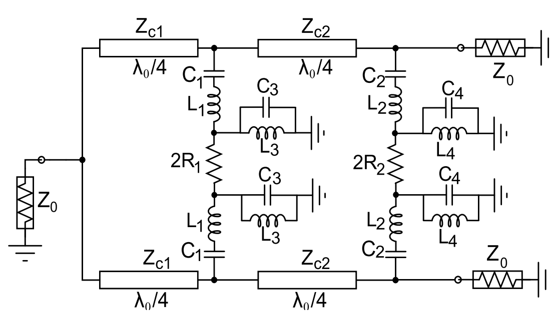

Figure 3.21: Two-section divider with the optimal isolation networks.

Table 3.2: Comparison Table

Reference	Technique	Size	Norm. BW	Loss (dB)
[6]	Microcoaxial Multisection	$6\lambda_0/4$	20-dB: 1.10	1
[43]	Multi Wafer Multisection	λ_0	15-dB: 1.15	1
[11]	Tapered Multisection	$5\lambda_0/6$	15-dB: 1.60	0.3
[8]	Three-section Coplanar Waveguide	$3\lambda_0/4$	15-dB: 1.15	0.8
[13]	Lumped Inductors	$\lambda_0/10$	20-dB: 0.15	0.3
[44]	Right-Left Handed isolation elements	$\lambda_0/4$	20-dB: 0.38	0.3
[45]	Single-section Trantanella	$\lambda_0/4$	20-dB: 0.36	0.2
[46]	Single-section Complex Termination	$\lambda_0/4$	20-dB: 0.15	0.1
[15]	Complex Isolation Components	$\lambda_0/4$	20-dB: 0.10	0.15
[22]	Single-section Modified Isolation Network	$\lambda_0/4$	18-dB: 0.40	0.5
This Work (Fig. 3.14)	Single-section Optimized Isolation Network	$\lambda_0/4$	20-dB: 0.68	0.2
This Work (Fig. 3.18)	Single-section Optimized Isolation Network	$\lambda_0/4$	19-dB: 0.75	0.2

Table 3.3: Normalized component values for input-output return losses and isolation better than δ (dB) for the divider in Fig. 3.21

δ	$\overline{\Delta f}$	$\overline{Z}_{c1}$	$\overline{Z}_{c2}$	$\overline{w_0 L_2}$	$\overline{w_0 L_3}$	$\overline{w_0 L_4}$	$2\overline{R}_1$	$2\overline{R}_2$
-20	1.15	1.60	1.25	0.68	–	6.88	1.97	3.36
-25	0.97	1.63	1.22	1.03	–	5.84	1.76	3.76
-30	0.80	1.66	1.21	1.30	26.8	5.30	1.74	4.25
-35	0.65	1.67	1.20	1.53	13	4.94	1.63	4.27
-40	0.53	1.67	1.19	1.65	10	4.77	1.46	3.94

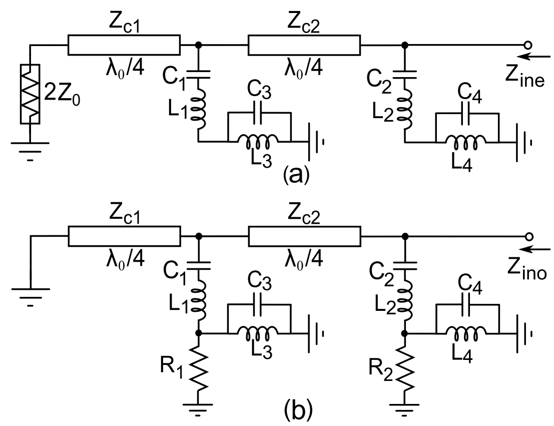

Figure 3.22: Even mode (a) and odd mode (b) equivalent circuits of the divider in Fig. 3.21.

Chapter 4

Directivity Enhancement Using S-Parameter Phase Relations

In this section, directivity and bandwidth performance of the microstrip directional couplers is explored in detail. Equations relating the phase difference between the coupling coefficient and isolation coefficient are derived. Using even-odd mode analysis, we show that the phase difference between the coupling factor and the isolation factor is close to π from DC up to the half wavelength frequency. Network analysis also yields that complex isolation factor and the coupling factor of a microstrip coupled line coupler lie along the same vector. This fact presents a high potential to achieve broadband directivity improvement through a voltage cancellation at the isolated port. Two coupler architectures are investigated for improvement. Using the proposed methods, the directivity bandwidth of couplers is significantly increased.

4.1 Even-Odd Mode Analysis

Consider a lossless symmetrical microstrip coupler shown in Fig. 4.1. We write the S-parameter matrix of the coupler as

$$\begin{bmatrix} b_1 \\ b_2 \\ b_3 \\ b_4 \end{bmatrix} = \begin{bmatrix} \Gamma & T & C & I \\ T & \Gamma & I & C \\ C & I & \Gamma & T \\ I & C & T & \Gamma \end{bmatrix} \begin{bmatrix} a_1 \\ a_2 \\ a_3 \\ a_4 \end{bmatrix} \tag{4.1}$$

where Γ, T, C, I are the reflection, transmission, coupling and isolation coefficients, respectively, all being complex numbers. This coupler can be analyzed

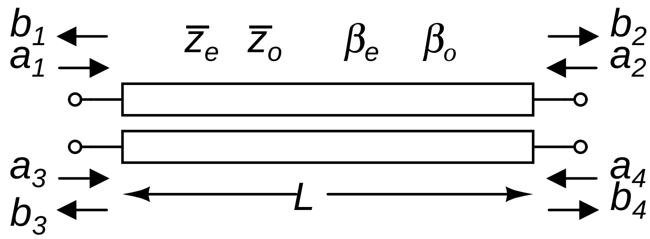

Figure 4.1: Microstrip coupler of length L with normalized even ($\overline{z}_e$) and odd ($\overline{z}_o$) mode characteristic impedances. β_e and β_o are even and odd mode propagation constants. a_i and b_i represent the incident and reflected wave amplitudes at port i.

using the even-odd mode analysis technique [24], [40], [49]. We can write

$$\Gamma = \frac{1}{4}(\Gamma_{ee} + \Gamma_{eo} + \Gamma_{oe} + \Gamma_{oo}) \tag{4.2}$$

$$C = \frac{1}{4}(\Gamma_{ee} + \Gamma_{eo} - \Gamma_{oe} - \Gamma_{oo}) \tag{4.3}$$

$$I = \frac{1}{4}(\Gamma_{ee} - \Gamma_{eo} - \Gamma_{oe} + \Gamma_{oo}) \tag{4.4}$$

where

$$\Gamma_{ee} = \frac{-j\overline{z}_e \cot(\beta_e L/2) - 1}{-j\overline{z}_e \cot(\beta_e L/2) + 1}\ ,\ \Gamma_{eo} = \frac{j\overline{z}_e \tan(\beta_e L/2) - 1}{j\overline{z}_e \tan(\beta_e L/2) + 1} \tag{4.5}$$

$$\Gamma_{oe} = \frac{-j\overline{z}_o \cot(\beta_o L/2) - 1}{-j\overline{z}_o \cot(\beta_o L/2) + 1}\ ,\ \Gamma_{oo} = \frac{j\overline{z}_o \tan(\beta_o L/2) - 1}{j\overline{z}_o \tan(\beta_o L/2) + 1} \tag{4.6}$$

$\overline{z}_e$ and $\overline{z}_o$ are the even and odd mode characteristic impedances of the coupled lines normalized with respect to Z_0 (the reference impedance for the S-parameters). β_e and β_o are the even and odd mode propagation constants of coupler of length L. β_e/β_o is assumed to be constant throughout the frequency range.[1] Moreover, we consider couplers with low coupling levels ($|C| < -10$ dB), so that $1 < \overline{z}_e < 1.4$ and $0.7 < \overline{z}_o < 1$.

Let f_1 be the frequency where $\beta_e L = \pi/4$ is satisfied, i.e., f_1 is the frequency where the coupler line length is equal to one eighth of the even-mode wavelength.

[1] Typically, this ratio does not vary more than 5% from the mean value [50]

For a better comprehension of the expressions (4.2), (4.3) and (4.4), we simplify them at specific frequencies: $f = 0$ and $f = 2f_1$.

4.1.1 For $f = 0$

Using Taylor expansion of (4.2) around $f = 0$ (i.e., for $f \ll f_1$) we find

$$\Gamma \approx j\frac{\pi}{16}\left(\frac{f}{f_1}\right)\left(\frac{\beta_o}{\beta_e}\overline{z}_o + \overline{z}_e - \frac{\beta_o}{\beta_e}\frac{1}{\overline{z}_o} - \frac{1}{\overline{z}_e}\right) \quad \text{for} \quad f \ll f_1 \tag{4.7}$$

Equating (4.7) to zero gives the optimal relationship between the parameters.

$$\frac{\overline{z}_o\beta_o + \overline{z}_e\beta_e}{\overline{z}_e\beta_o + \overline{z}_o\beta_e}\overline{z}_o\overline{z}_e = 1 \tag{4.8}$$

If $\beta_e = \beta_o$, we must choose $\overline{z}_e\overline{z}_o = 1$ to satisfy the condition. On the other hand, if $\beta_e > \beta_o$ which is the case for microstrip coupled lines, we find that $\overline{z}_e\overline{z}_o < 1$. $\overline{z}_e$ can be explicitly written in terms of $\overline{z}_o$ and $b = \beta_e/\beta_o$ as

$$\overline{z}_e = \frac{1}{2b}\left[\left(\frac{1}{\overline{z}_o^2} + 4b^2 - 2 + \overline{z}_o^2\right)^{\frac{1}{2}} + \frac{1}{\overline{z}_o} - \overline{z}_o\right] \tag{4.9}$$

Alternatively, we can express b in terms of $\overline{z}_e$ and $\overline{z}_o$ under optimal condition of (4.8) as

$$b = \frac{(1 - \overline{z}_o^2)\overline{z}_e}{(\overline{z}_e^2 - 1)\overline{z}_o} \tag{4.10}$$

We can write the first two terms of the Taylor series around $f = 0$ for the complex coupling and isolation coefficients as

$$\begin{aligned} C \;\approx\;& j\frac{\pi}{16}\left(\frac{f}{f_1}\right)\left(\overline{z}_e - \frac{1}{\overline{z}_e} - \frac{\overline{z}_o}{b} + \frac{1}{b\overline{z}_o}\right) \\ &+\frac{\pi^2}{128}\left(\frac{f}{f_1}\right)^2\left(\overline{z}_e^2 - \frac{1}{\overline{z}_e^2} + \frac{1}{b^2\overline{z}_o^2} - \frac{\overline{z}_o^2}{b^2}\right) \end{aligned} \tag{4.11}$$

$$\begin{aligned} I \;\approx\;& -j\frac{\pi}{16}\left(\frac{f}{f_1}\right)\left(\overline{z}_e + \frac{1}{\overline{z}_e} - \frac{\overline{z}_o}{b} - \frac{1}{b\overline{z}_o}\right) \\ &-\frac{\pi^2}{128}\left(\frac{f}{f_1}\right)^2\left(\overline{z}_e^2 + \frac{1}{\overline{z}_e^2} - \frac{1}{b^2\overline{z}_o^2} - \frac{\overline{z}_o^2}{b^2}\right) \end{aligned} \tag{4.12}$$

Directivity for $f \ll f_1$, $D_0 = |C/I|$, can be written as

$$D_0 \approx \frac{b\overline{z}_e - b/\overline{z}_e - \overline{z}_o + 1/\overline{z}_o}{b\overline{z}_e + b/\overline{z}_e - \overline{z}_o - 1/\overline{z}_o} \tag{4.13}$$

The phase difference between the coupling and isolation coefficients is given by

$$(\angle C - \angle I) \approx \pi + \frac{\pi}{4} AB \frac{A' - B'}{A^2 - B^2} \left(\frac{f}{f_1}\right) \quad \text{for} \quad f \ll f_1 \tag{4.14}$$

with

$$A = b\overline{z}_e - \overline{z}_o, \;\; A' = \overline{z}_e + \frac{\overline{z}_o}{b} \tag{4.15}$$

$$B = \frac{1}{\overline{z}_o} - \frac{b}{\overline{z}_e}, \;\; B' = \frac{1}{b\overline{z}_o} + \frac{1}{\overline{z}_e} \tag{4.16}$$

In (4.14), the term in front of (f/f_1) vanishes for $B = 0$ or $A' = B'$. These imply

$$\frac{\overline{z}_e}{\overline{z}_o} = b \quad \text{or} \quad \frac{\overline{z}_o + b\overline{z}_e}{\overline{z}_e + b\overline{z}_o} \overline{z}_o \overline{z}_e = 1 \tag{4.17}$$

The second condition in (4.17) is the same as (4.8) so we have $|\Gamma| \approx 0$ and $(\angle C - \angle I) \approx \pi$. Even if (4.17) is not exactly satisfied, (4.14) still predicts a phase very close to π since $(A' - B') \ll 1$.

4.1.2 For $f = 2f_1$

At this frequency we have $\beta_e L = \pi/2$. Hence, $\tan(\beta_o L/2) = \tan(\pi/4 - (\beta_e - \beta_o)L/2) \approx 1 - (\beta_e - \beta_o)L$ with comparable β_e and β_o. In this case (4.5) and (4.6) reduce to

$$\Gamma_{ee} = \frac{-j\overline{z}_e - 1}{-j\overline{z}_e + 1} \;, \; \Gamma_{eo} = \frac{j\overline{z}_e - 1}{j\overline{z}_e + 1} \tag{4.18}$$

$$\Gamma_{oe} \approx \frac{-j\overline{z}_o(1+\xi) - 1}{-j\overline{z}_o(1+\xi) + 1} \;, \; \Gamma_{oo} \approx \frac{j\overline{z}_o(1-\xi) - 1}{j\overline{z}_o(1-\xi) + 1} \tag{4.19}$$

where $\xi = (\beta_e - \beta_o)L = (\pi/2)(b-1)/b$. Combining (4.18) and (4.19) with (4.3) and (4.4), the ratio of the coupling coefficient to the isolation coefficient can be written as:

$$\frac{C}{I} \approx -\frac{\overline{z}_e^2 - \overline{z}_o^2}{2\xi \; \overline{z}_e\overline{z}_o + j(\overline{z}_e - \overline{z}_o)(1 - \overline{z}_e\overline{z}_o)} \tag{4.20}$$

So, the phase difference at $f = 2f_1$ equals:

$$\angle C - \angle I \approx \pi - \tan^{-1}\left(\frac{(\overline{z}_e - \overline{z}_o)(1 - \overline{z}_e\overline{z}_o)}{2\xi \; \overline{z}_e\overline{z}_o}\right) \tag{4.21}$$

Using (4.10) and $\xi = (\pi/2)(b-1)/b$, (4.21) can be rewritten as

$$\angle C - \angle I \approx \pi - \tan^{-1}\left(\frac{(1 - \overline{z}_o^2)(\overline{z}_e - \overline{z}_o)}{\pi\overline{z}_o(\overline{z}_e + \overline{z}_o)}\right) \approx \pi \tag{4.22}$$

since $(1-\overline{z}_o^2)(\overline{z}_e-\overline{z}_o) \ll \pi\overline{z}_o(\overline{z}_e+\overline{z}_o)$. With low coupling levels, the error term is even smaller. For example, for a 10 dB coupler with $b = 1.1$, (4.22) gives a phase difference of $\pi - 0.022\pi$, for a 30 dB coupler with $b = 1.1$ the result is $\pi - 0.0002\pi$. Hence the imaginary term in the denominator of (4.20) can be ignored, and we find the directivity, D_2, at $f = 2f_1$ as:

$$D_2 = \left|\frac{C}{I}\right| \approx \frac{1}{\pi}\frac{b}{b-1}\left(\frac{\overline{z}_e}{\overline{z}_o} - \frac{\overline{z}_o}{\overline{z}_e}\right) \tag{4.23}$$

which is smaller than D_0.

A numerical evaluation of (4.3) and (4.4) as depicted in Fig. 4.2 shows that $(\angle C - \angle I) \approx \pi$ approximation is actually valid along a wide range: $0 \leq f < 4f_1$. It is possible to reach a similar conclusion using the network theory (See Appendix-A). Hence we can write in this frequency range

$$D = \left|\frac{C}{I}\right| = -\frac{C}{I} \tag{4.24}$$

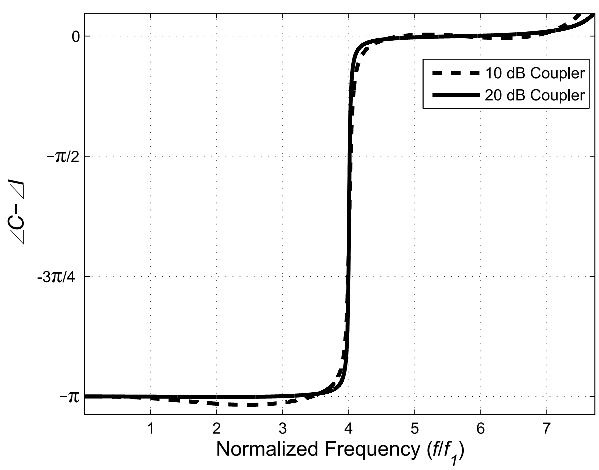

Figure 4.2: Phase difference (in radians) between coupling and isolation factors for two couplers specified in Table 4.1.

Table 4.1 lists the specifications of two couplers that are used in examples. W and S are the width and spacing of the lines. $b = \beta_e/\beta_o$ ratios are extracted using

Table 4.1: Example Couplers

Coupling	10 dB	20 dB
$b = \beta_e/\beta_o$	1.105	1.073
$\overline{z_e}$	1.365	1.10
$\overline{z_o}$	0.709	0.90
Implementation $e_r = 3.55$, $h = 0.8$ mm	$W = 1.53$ mm $S = 0.125$ mm	$W = 1.79$ mm $S = 0.99$ mm

a microwave circuit simulator[2] considering a representative dielectric permittivity of e_r=3.55 and substrate thickness of 0.8 mm. $\overline{z_e}$ and $\overline{z_o}$ are calculated using (4.8) and the prescribed coupling level. For the 10dB coupler, the theoretical phase deviation of $\angle C - \angle I$ from π is less than 4.2° in $0 \leq f < 3.8f_1$. For the 20dB coupler, the error is smaller than 0.27° in $0 \leq f < 3.2f_1$.

4.2 Application of the Phase Relations

The inherent π phase difference between C and I in a wide frequency range can be used to achieve broadband directivity by a cancellation at the isolated port of the couplers. Two methods are explored in the following sections. Short length couplers [37],[51] are utilized as the directivity characteristic is relatively constant for the frequencies lower than the quarter wavelength frequency.

4.2.1 Reflected Power Cancellation

In a conventional coupler, the directivity is highly deteriorated by the unmatched loads at the outputs. This condition is generally faced when one desires to monitor forward and reverse power values using detector circuits at the coupled and isolated ports. If the input reflection of the detectors is not low enough, the directivity is severely reduced. For example, the directivity of a 20 dB coupler may easily degrade to 12 dB if the load connected to the coupled port has a return loss of 16 dB. A common solution for this problem is to use two separate couplers, one for the forward, the other for reverse power measurements. Unused ports are terminated perfectly not to degrade the directivity.

[2] AWR Corp. El Segundo, CA 90245, USA, http://www.awrcorp.com

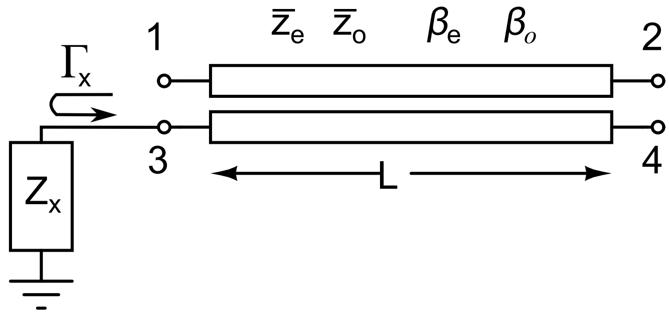

Figure 4.3: Coupler with an unmatched load of Z_x at port 3 to improve directivity at port 4 using reflected power cancellation scheme.

On the other hand, if the termination of the unused port is properly chosen, the isolation can be improved. The technique was used in [33] and [34] and narrowband directivity peaks were obtained. In what follows, we present how a broadband directivity improvement can be obtained.

Referring to Fig. 4.3 and (4.1), suppose $a_1 = 1$, $a_2 = 0$, $a_4 = 0$ and that the coupled port is terminated with a load of reflection coefficient Γ_x such that $a_3 = \Gamma_x b_3$. We can write the modified reflection, $\Gamma_m = b_1/a_1$, as

$$\Gamma_m \approx \Gamma + C^2\Gamma_x \approx \Gamma \tag{4.25}$$

since $|C|^2$ is small. The modified isolation, $I_m = b_4/a_1$, is given by

$$I_m \approx I + C\Gamma_x e^{-j\beta L} \tag{4.26}$$

Here, the effective propagation constant β can be expressed in terms of β_e using the relations between the effective dielectric permittivity and the even odd mode permittivities given in [52]:

$$\beta = \frac{\beta_e + \beta_o}{2} = \beta_e(\frac{b+1}{2b}) \tag{4.27}$$

(4.26) reveals that the isolation can be improved considerably if Γ_x can be chosen such that:

$$\Gamma_x \approx -\frac{Ie^{j\beta L}}{C} \approx \frac{e^{j\beta L}}{D} \tag{4.28}$$

where (4.24) is utilized.

By choosing $a_1 = 0$, $a_2 = 1$, $a_3 = \Gamma_x b_3$ and $a_4 = 0$, the modified coupling factor, $C_m = b_4/a_2 = b_4$, is found as

$$C_m \approx C + I\Gamma_x e^{-j\beta L} = C\left(1 - \frac{I^2}{C^2}\right) \approx C \tag{4.29}$$

since $|I/C|^2 = 1/D^2 \ll 1$. We note that in the modified coupler of Fig. 4.3, the phase difference between C_m and I_m is no longer π.

Realization of (4.28) requires an amplitude response in the form of $1/D$ in addition to the linear phase term. The couplers with a minimized input return loss have a monotonic decreasing directivity characteristic as shown in Fig. 4.4. The load impedance shown in Fig. 4.5 is a good choice to approximately satisfy (4.28).

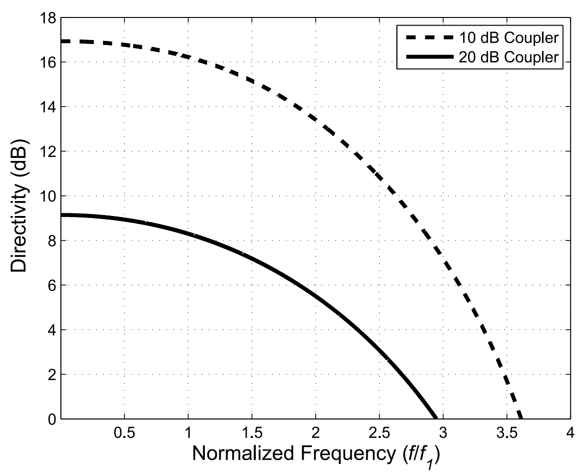

Figure 4.4: Directivity characteristic of the two couplers specified in Table 4.1.

The values of the components in Fig. 4.5 can be found by equating the impedance of the proposed load to the desired load at two frequencies, $f = 0$ and $f = f_a$. The impedance at $f = 0$ is a pure resistance. The directivity, D_0, at $f = 0$ is expressed in (4.13). So, we can find the required normalized resistor, $\overline{R}_x = R_x/Z_0$ as

$$\overline{R}_x = \frac{1 + 1/D_0}{1 - 1/D_0} = \frac{b\overline{z}_e - \overline{z}_o}{1/\overline{z}_o - b/\overline{z}_e} \tag{4.30}$$

Equating the impedances at $f = f_a$ ($\omega = \omega_a$)

$$\left.\frac{1 + e^{j\beta L}/D_a}{1 - e^{j\beta L}/D_a}\right|_{f=f_a} = \frac{\overline{R}_x - \overline{\omega_a L}_x\,\overline{\omega_a C}_x\,\overline{R}_x + j\overline{\omega_a L}_x}{1 + j\overline{\omega_a C}_x\,\overline{R}_x} \tag{4.31}$$

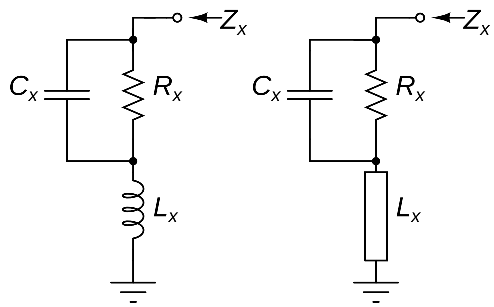

Figure 4.5: Lumped element and distributed element versions of proposed circuit for Z_x. (L_x can be approximated by a shorted transmission line.)

where D_a is the directivity at f_a. At $f = f_a$, $\beta L = \pi f_a(b+1)/8f_1b$. The normalized susceptance $\overline{\omega_a C_x} = Z_0\omega_a C_x$ and reactance $\overline{\omega_a L_x} = \omega_a L_x/Z_0$ can be calculated by equating the real and imaginary parts of (4.31) at $f = f_a$:

$$\overline{\omega_a C_x} = \frac{1}{\overline{R}_x}\sqrt{\frac{\overline{R}_x(D_a^2 - 2D_a\cos\theta_a + 1)}{D_a^2 - 1} - 1} \tag{4.32}$$

$$\overline{\omega_a L_x} = \frac{2D_a\sin\theta_a}{D_a^2 - 2D_a\cos\theta_a + 1} + \frac{\overline{\omega_a C_x}\,\overline{R}_x^2}{1 + \overline{\omega_a C}_x^2\overline{R}_x^2} \tag{4.33}$$

with $\theta_a = \pi f_a(b+1)/8f_1b$.

f_a is varied to get differing amounts of improvement in the directivity. Smaller values of f_a give higher directivity but a small bandwidth. Larger values of f_a result in a lower directivity with a larger bandwidth. Fig. 4.6 shows the resulting normalized bandwidth, f_B/f_1, for two different coupling levels as a function of the obtained directivity. Directivity is specified as the minimum value in the frequency range $0 < f < f_B$. Fig. 4.7 depicts the required component values to achieve the desired directivity for the same couplers. For example, for the 10 dB coupler, the directivity is at least 35 dB in the frequency range $0 < f < 1.45f_1$ using components $\overline{R}_x$=1.33, $\overline{\omega_1 L_x}$=0.6 and $1/\overline{\omega_1 C_x}$=4.4.

4.2.2 Forward Power Cancellation

Another technique suitable for bandwidth enhancement through the results of the phase difference analysis is the forward power cancellation. An attenuated

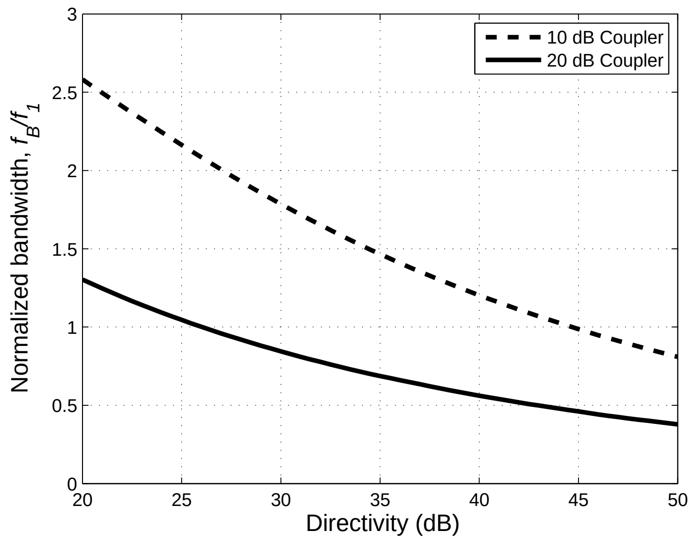

Figure 4.6: Normalized bandwidth (f_B/f_1) versus directivity with reflected power cancellation technique for the couplers specified in Table 4.1. Directivity is satisfied within the frequency band $0 < f < f_B$.

version of the coupled signal is forwarded to the isolated port to cancel the signal there. The method was used in [35, 36], however the directivity improvement in both works was narrowband. A wideband cancellation is possible as described below.

Fig. 4.8 shows the proposed structure where an equalizer is implemented using a π-attenuator with an inductor in one of the arms. The other arm of the attenuator does not have the inductor to keep the input return loss high, since a reflection may reduce the directivity. At high frequencies a properly chosen inductor L_1 reduces the attenuation to mimic the desired directivity versus frequency characteristics. The extra phase introduced by the equalizer is compensated by unequal length transmission lines, l_1 and l_2. Three resistors of value $R_3 = Z_0/3$ are utilized to combine the signals at port 3.

Let T_1 be the frequency dependent complex transmission coefficient of the equalizer and Γ_1 and Γ_2 be the reflection coefficients as shown in Fig. 4.8. If $|\Gamma_1| \ll |T_1|$, the modified isolation coefficient, $I'_m = b_3/a_1$, is given by

$$I'_m \approx (Ie^{-j\beta l_2} + CT_1 e^{-j\beta l_1})/2 \qquad (4.34)$$

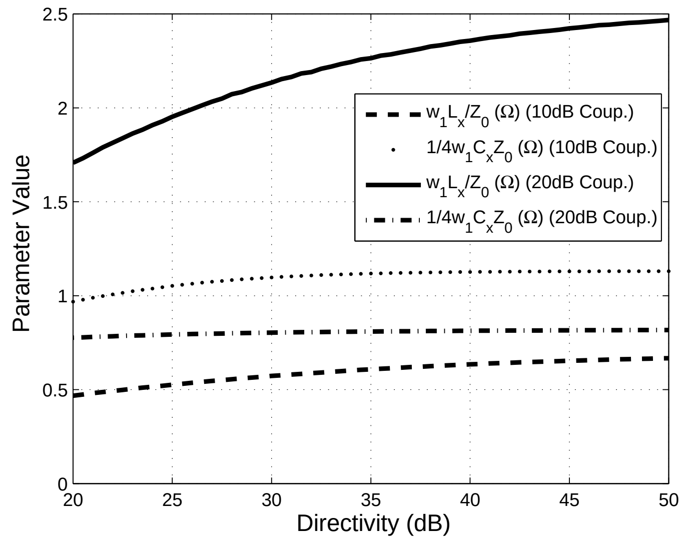

Figure 4.7: Normalized reactance values using (4.32) and (4.33) to achieve the required directivity in Fig. 4.6 for two couplers. The normalized reactance values are specified at $f_1 = \omega_1/2\pi$. The capacitive reactance is scaled by 1/4. R_x/Z_0 is 1.33 for the 10 dB coupler and 2.07 for the 20 dB coupler.

where 1/2 factor is due to the power combining circuit. So, the required transmission coefficient to nullify I'_m is:

$$T_1 = \frac{e^{j\beta(l_1-l_2)}}{D} \tag{4.35}$$

Similarly, the modified coupling coefficient, $C'_m = b_3/a_2$, can be expressed as

$$C'_m = (Ce^{-j\beta l_2} + IT_1e^{-j\beta l_1})/2 \approx Ce^{-j\beta l_2}/2 \tag{4.36}$$

since we have $|T_1| = 1/D$ from (4.35) and $|IT_1| \ll |C|$. In other words, the coupling of the forward cancellation scheme is 6 dB lower than the original coupler. Considering only the first order reflections, the modified input reflection coefficient, $\Gamma'_m = b_1/a_1$, can be expressed as

$$\Gamma'_m \approx \Gamma + C^2\Gamma_1 + I^2\Gamma_2 \approx \Gamma \tag{4.37}$$

where the last approximation is due to small $|\Gamma_1|$, $|\Gamma_2|$, C^2 and I^2 terms.

Similar to the previous technique, we impose perfect directivity at $f = 0$ and $f = f_a$. At $f = 0$, the equalizer is a pure attenuator. The values of the required

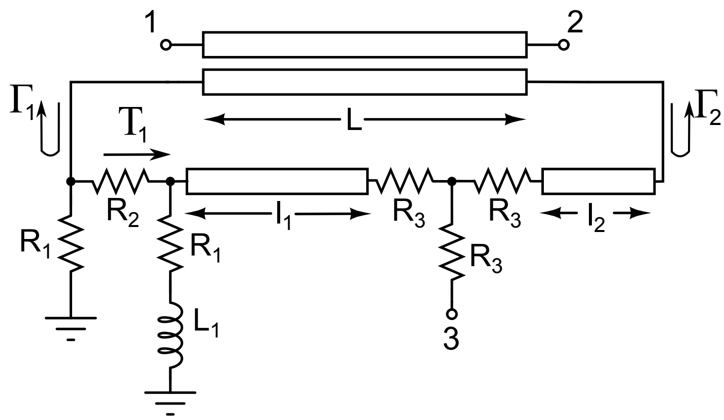

Figure 4.8: Coupler with improved directivity at port 3 using forward power cancellation scheme.

resistors can be formulated considering that the attenuation level should be equal to $1/D_0$. The normalized resistor values are

$$\overline{R_1} = \frac{1 + 1/D_0}{1 - 1/D_0} \tag{4.38}$$

$$\overline{R_2} = \frac{D_0^2 - 1}{2D_0} \tag{4.39}$$

where D_0 is given by (4.13). The value of L_1 and the length difference $l_1 - l_2$ can be found by the conditions at $f = f_a$. The normalized reactance, $\overline{\omega_a L_1}$ is found as

$$\overline{\omega_a L_1} = \sqrt{\frac{(\overline{R}_1 + \overline{R}_2 + \overline{R}_1\ \overline{R}_2)^2 - D_a^2 \overline{R}_1{}^2}{D_a^2 - (1 + \overline{R}_2)^2}} \tag{4.40}$$

where D_a is the uncompensated directivity at $f = f_a$. $\beta(l_1 - l_2)$ is the phase difference necessary to compensate the positive phase caused by L_1 specified at f_a

$$\beta(l_1 - l_2) = \tan^{-1}\left(\frac{\overline{\omega_a L_1}}{\overline{R}_1}\right) - \tan^{-1}\left(\frac{\overline{\omega_a L_1}(1 + \overline{R}_2)}{\overline{R}_1 + \overline{R}_2 + \overline{R}_1\ \overline{R}_2}\right) \tag{4.41}$$

The couplers listed in Table 4.1 are simulated to check the bandwidth capability of the forward power cancellation technique. The results are shown in Fig. 4.9. A better performance is obtained compared to the reflected power cancellation scheme. For example, the directivity of the 10 dB coupler can be increased to

35 dB in the frequency range $0 < f < 1.85f_1$. Fig. 4.10 shows the component values to achieve the required directivity.

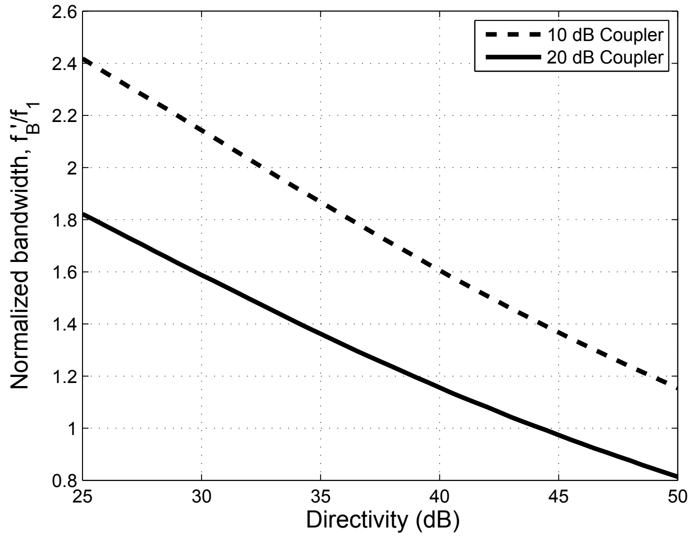

Figure 4.9: Normalized bandwidth (f'_B/f_1) versus directivity with forward power cancellation technique for the couplers specified in Table 4.1. Directivity is satisfied within the frequency band $0 < f < f'_B$.

4.3 Experimental Results

Couplers are designed and implemented for experimental verification. RO4003[3] substrate with a thickness of 0.8 mm is used with a coupled section length of L=20 mm (f_1=1.12 GHz) and a gap of W=0.3 mm. Coupled lines are added on both sides of the main line[4] to get independent coupled and isolated ports as depicted in Fig. 4.11. For input at port 1, the coupled port is #3 and the isolated port is #4. For this coupler z_e=62Ω, z_o=39.4Ω, $b = 1.098$, D_0=14dB and $|C| = -13$dB at $f = 2f_1$. Fig. 4.12 shows the calculated (from (4.3) and (4.4)) and measured phase differences between the coupling (S_{31}) and the isolation

[3]Rogers Corp. Rogers, CT 06263, USA, http://www.rogerscorp.com

[4]Since the coupling is weak, analytical results of previous sections are also valid for this three-line coupler.

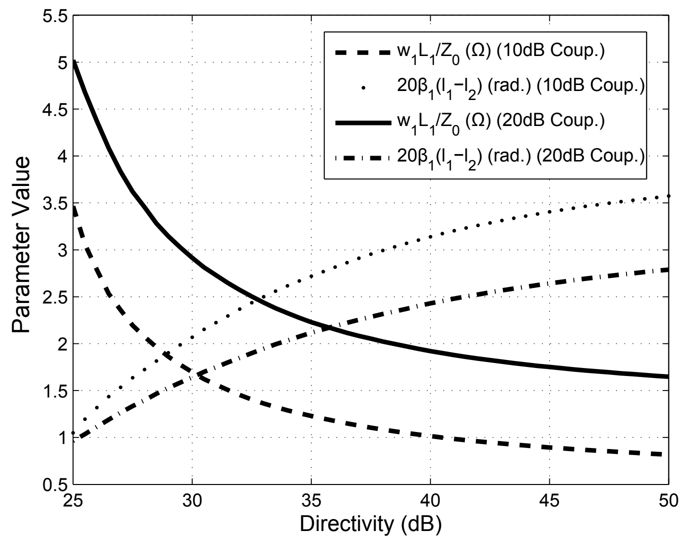

Figure 4.10: Normalized values to achieve the directivity for two couplers using the forward power cancellation scheme shown in Fig. 4.8. The reactance and phase values are specified at f_1. The phase value is scaled by 20 to improve readability. $\overline{R_1}, \overline{R_2}$, respectively are 1.33, 3.44 for the 10 dB coupler and 2.072, 1.258 for the 20 dB coupler.

(S_{32}). The variation in the measured phase difference is higher than expected, possibly because of the small reflections at 90° bends and at the termination resistor in the isolation measurement.

The reflected power and the forward power cancellation schemes are implemented as shown in Fig. 4.13. The component values are found from the equations of Section-III. With less ambitious directivity goals, these values can be used directly. But for higher directivity values, a modification in values is necessary to take care of the parasitic effects such as transmission line bends, junction discontinuities, via hole inductors, unintended couplings and the parasitics of the lumped elements. An optimization is performed using the microwave circuit simulator and an electromagnetic simulator[5] for the final values.

For the reflected power cancellation scheme, the coupler is designed to give a directivity of 40dB. For this directivity target, we estimate from Fig. 4.6 a bandwidth

[5] SONNET Software, North Syracuse NY 13212, USA, http://www.sonnetsoftware.com

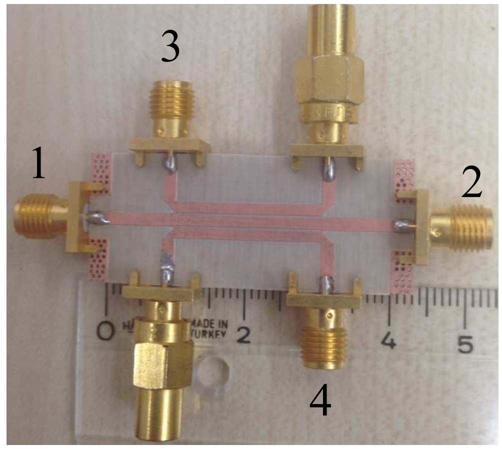

Figure 4.11: Photo of the original microstrip coupler.

of $f_B = 0.9f_1$=1GHz. Component values of the termination can be calculated from (4.30), (4.32) and (4.33) as R_x=74.8Ω, $C_x = 0.73$pF and $L_x = 7.3$nH. The component values of R_x=75Ω and C_x=0.70pF are used at the experimental step. L_x is realized with a microstrip line of 0.6mm width and 10mm length.

For the forward power cancellation technique, Fig. 4.9 predicts a bandwidth of $f'_B = 1.5f_1$ =1.7GHz for a directivity of 40dB. From (4.38), (4.39), (4.40), (4.41), the required component values are R_1=74.8Ω, R_2=121Ω, L_1=8.5nH and $\beta_1(l_1 - l_2)$=0.15 implying $l_1 - l_2$=3.8 mm. Following the optimization, the component values are modified. In the experimental step, 75Ω–178Ω–82.5Ω resistor combination results in a better directivity response. L_1 is realized with a shorted microstrip line of 0.8 mm width and 13 mm length.

Simulated directivity responses are displayed in Fig. 4.14 verifying the predicted f_B and f'_B values for both schemes. Fig. 4.15 presents the coupling responses. We note that the coupling value itself is not constant for f less than f_B or f'_B, a characteristic of short length couplers [51]. In this frequency range, the coupling of the reflected cancellation scheme follows that of the original coupler, while the coupling of the forward power cancellation case is approximately 6dB lower as expected. The simulated input return losses of the reflected and the forward cancellation schemes are close to the original one as seen in Fig. 4.16. The insertion losses are better than 0.5 dB for both cases.

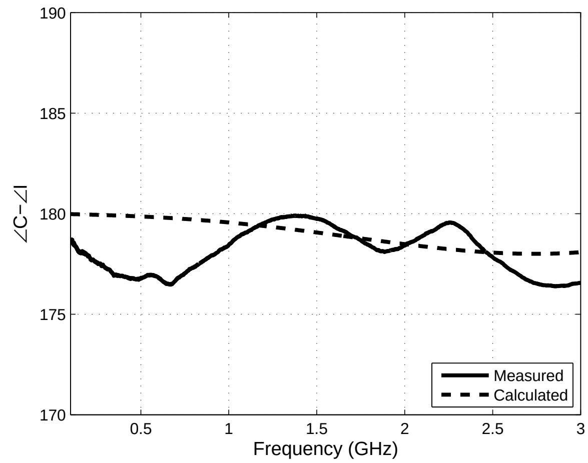

Figure 4.12: Calculated and measured phase differences (in degrees) between the coupling and the isolation for the original coupler.

Measured directivity responses are given in Fig. 4.17. The reflected power cancellation scheme has directivity of 40 dB in the band $0 < f < 0.9$ GHz. On the other hand, the forward power cancellation method gives the same directivity in the band $0 < f < 1.7$ GHz. Fig. 4.18 and 4.19 show the measured coupling, return loss and insertion loss responses. The measurements are in good agreement with the simulation results.

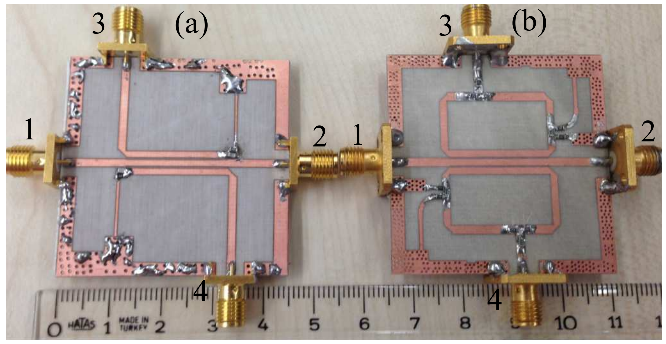

Figure 4.13: Photo of the couplers with reflected power cancellation and forward power cancellation schemes.

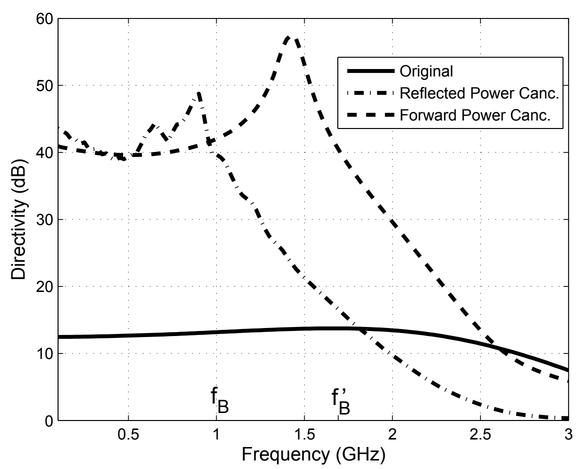

Figure 4.14: Directivity of the original, reflected power cancellation and forward power cancellation schemes as found by the microwave circuit simulator.

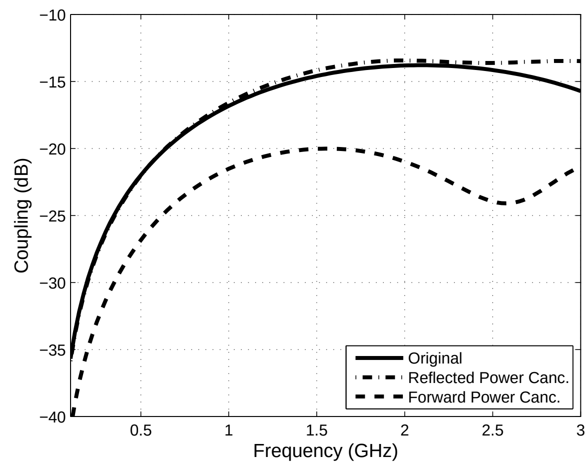

Figure 4.15: Coupling of the original, reflected power cancellation and forward power cancellation schemes as found by the microwave circuit simulator.

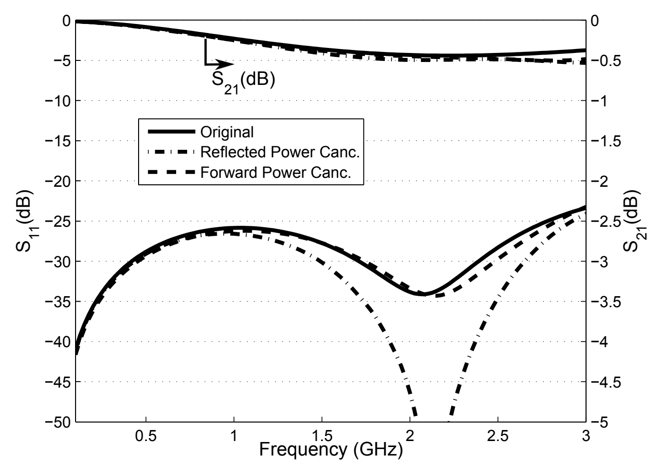

Figure 4.16: Return loss and insertion loss characteristics of the original, reflected power cancellation and forward power cancellation schemes as found by the microwave circuit simulator.

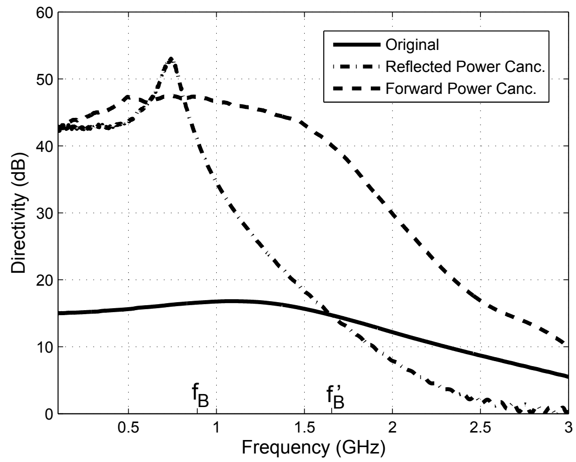

Figure 4.17: Measured directivity of the original, reflected power cancellation and forward power cancellation schemes.

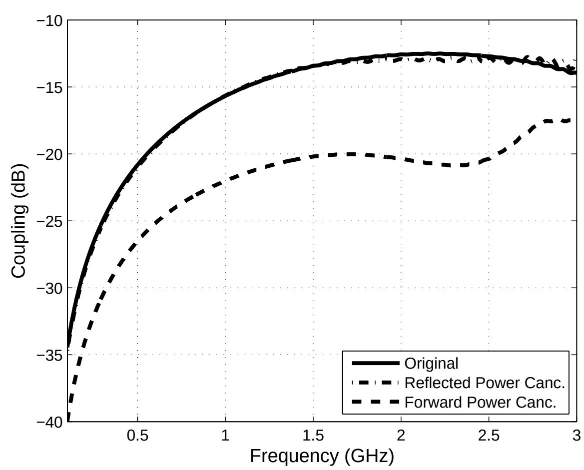

Figure 4.18: Measured coupling of the original, reflected power cancellation and forward power cancellation schemes.

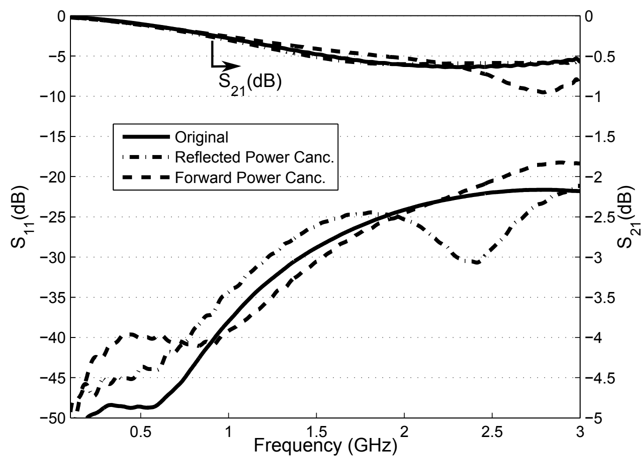

Figure 4.19: Measured return loss and insertion loss characteristic of the original, reflected power cancellation and forward power cancellation schemes.

Chapter 5

Conclusions

We derived S-parameter expressions applicable to several kinds of power dividers and directional couplers. The expressions for the power dividers relate input-output return losses and isolation values. When a general power divider is considered, the expression involves only the magnitudes of S-parameters. When we consider a special power divider, namely the Wilkinson divider, the S-parameter relations are more strict and they relate the complex-valued S-parameters. The equations can be used to reduce the number of variables in the parameter optimization problems. Starting from a fundamental S-parameter relation of a lossless power divider, we find that minimizing the even and odd mode reflection coefficients of an output port is sufficient to optimize a power divider. Using this fact, we are able to synthesize even and odd mode isolation networks to maximize the bandwidth of a single-section Wilkinson divider. The reflection coefficients of the isolation network that perfectly match the even and odd mode circuits are calculated individually. Then, circuits are designed to realize the required reflection coefficients. The even mode and odd mode isolation networks are merged in a configuration to load each other minimally. Analytical expressions are derived for the component values of those networks. The resulting divider has a considerably wider operation bandwidth compared to the classical Wilkinson divider. Experimental verification is presented proving that the proposed low-loss divider is promising for wide band applications. The method can be applied to a two-section divider. Using a similar isolation arm for both sections, it is possible to extend the bandwidth considerably. The S-parameter expression for the directional coupler relate the phases of isolation and coupling coefficients. An interesting result is achieved. It is shown that the phase difference between the coupling and the isolation coefficients is very close to π in a wide band. This characteristic is suitable for directivity enhancement using two different methods proposed in this work. The required component values for both methods can be calculated by the given analytical expressions. Verified also by experimental results, both methods increase the directivity of the microstrip directional coupler in a wide bandwidth.

Bibliography

[1] S. Cohn, "A class of broadband three-port TEM-mode hybrids," *IEEE Trans. Microw. Theory Techn.*, vol. 19, pp. 110–116, Feb. 1968.

[2] J. Reed and G. Wheeler, "A method of analysis of symmetrical four-port networks," *IRE Trans. Microw. Theory Techn.*, vol. 4, pp. 246 –252, Oct. 1956.

[3] E. Wilkinson, "An N-way hybrid power divider," *IEEE Trans. Microw. Theory Techn.*, vol. 8, pp. 116–118, Jan. 1960.

[4] R. Ekinge, "A new method of synthesizing matched broad-band TEM-mode three-ports," *IEEE Trans. Microw. Theory Techn.*, vol. 19, pp. 81 – 88, Jan. 1971.

[5] H. Oraizi and A.-R. Sharifi, "Design and optimization of broadband asymmetrical multisection Wilkinson power divider," *IEEE Trans. Microw. Theory Techn.*, vol. 54, pp. 2220–2231, May. 2006.

[6] N. Ehsan, K. Vanhille, S. Rondineau, E. Cullens, and Z. Popovic, "Broadband micro-coaxial Wilkinson dividers," *IEEE Trans. Microw. Theory Techn.*, vol. 57, pp. 2783–2789, Nov. 2009.

[7] J.-C. Chieh and A.-V. Pham, "Development of a broadband Wilkinson power combiner on liquid crystal polymer," in *Proc. Asia Pacific Microw. Conf.*, pp. 2068–2071, Dec. 2009.

[8] J.-S. Lim, U.-H. Park, S. Oh, J. J. Koo, Y.-C. Jeong, and D. Ahn, "A 800- to 3200-mhz wideband cpw balun using multistage Wilkinson structure," in *IEEE MTT-S Int. Microw. Symp. Dig.*, pp. 1141–1144, June 2006.

[9] S. Wong and L. Zhu, "Ultra-wideband power dividers with good isolation and improved sharp roll-off skirt," *IET Microw. Antennas Propag.*, vol. 3, pp. 1157–1163, Dec. 2009.

[10] P. Goodman, "A wideband stripline matched power divider," in *G-MTT International Microwave Symposium*, pp. 16–20, May. 1968.

[11] C. T. Chiang and B.-K. Chung, "Ultra wideband power divider using tapered line," in *Progress In Electromagnetics Research*, vol. 106, pp. 61–73, 2010.

[12] K. Hettak, G. Morin, and M. Stubbs, "Compact mmic cpw and asymmetric cps branch-line couplers and Wilkinson dividers using shunt and series stub loading," *IEEE Trans. Microw. Theory Techn.*, vol. 53, pp. 1624–1635, May. 2005.

[13] R. Mirzavand, M. Honari, A. Abdipour, and G. Moradi, "Compact microstrip Wilkinson power dividers with harmonic suppression and arbitrary power division ratios," *IEEE Trans. Microw. Theory Techn.*, vol. 61, pp. 61–68, Jan. 2013.

[14] Y.-S. Lin and J.-H. Lee, "Miniature ultra-wideband power divider using bridged t-coils," *IEEE Microw. Compon. Lett.*, vol. 22, pp. 391–393, Aug. 2012.

[15] X. Wang, I. Sakagami, A. Mase, and M. Ichimura, "Wilkinson power divider with complex isolation component and its miniaturization," *IEEE Trans. Microw. Theory Techn.*, vol. 62, pp. 422–430, Mar. 2014.

[16] T. Kawai, J. Yamasaki, Y. Kokubo, and I. Ohta, "A design method of dual-frequency Wilkinson power divider," in *Proc. Asia Pacific Microw. Conf.*, pp. 913–916, 2006.

[17] X. Wang and I. Sakagami, "Generalized dual-frequency Wilkinson power dividers with a series/parallel rlc circuit," in *IEEE MTT-S Int. Microw. Symp. Dig.*, pp. 1–4, June 2011.

[18] Y. Wu, Y. Liu, and S. Li, "Unequal dual-frequency Wilkinson power divider including series resistor-inductor-capacitor isolation structure," *IET Microw. Antennas Propag.*, vol. 3, no. 7, pp. 1079–1085, 2009.

[19] Y. Wu, Y. Liu, and Q. Xue, "An analytical approach for a novel coupled-line dual-band Wilkinson power divider," *IEEE Trans. Microw. Theory Techn.*, vol. 59, pp. 286–294, Feb. 2011.

[20] Y. Wu, Y. Liu, Y. Zhang, J. Gao, and H. Zhou, "A dual band unequal Wilkinson power divider without reactive components," *IEEE Trans. Microw. Theory Techn.*, vol. 57, pp. 216–222, Jan. 2009.

[21] A. Genc and R. Baktur, "Dual- and triple-band Wilkinson power dividers based on composite right- and left-handed transmission lines," *IEEE Trans. Compon. Packag. Manuf. Technol.*, vol. 1, pp. 327–334, Mar. 2011.

[22] J.-C. Kao, Z.-M. Tsai, K.-Y. Lin, and H. Wang, "A modified Wilkinson power divider with isolation bandwidth improvement," *IEEE Trans. Microw. Theory Techn.*, vol. 60, pp. 2768–2780, Sep. 2012.

[23] S.-F. Chao and Y.-R. Li, "Miniature filtering power divider with increased isolation bandwidth," *Electronics Letters*, vol. 50, pp. 608–610, Apr. 2014.

[24] I. B. R. Mongia and P. Bhartia, *RF and Microwave Coupled-Line Circuits.* Boston, MA: Artech House, 1999.

[25] A. Podell, "A high directivity microstrip coupler technique," in *Microwave Symposium, G-MTT 1970 International*, pp. 33–36, May 1970.

[26] B. Sheleg and B. Spielman, "Broad-band directional couplers using microstrip with dielectric overlays," *Microwave Theory and Techniques, IEEE Transactions on*, vol. 22, pp. 1216–1220, Dec. 1974.

[27] J. Klein and K. Chang, "Optimum dielectric overlay thickness for equal even- and odd-mode phase velocities in coupled microstrip circuits," *Electronics Letters*, vol. 26, pp. 274–276, Mar. 1990.

[28] M. Dydyk, "Microstrip directional couplers with ideal performance via single-element compensation," *Microwave Theory and Techniques, IEEE Transactions on*, vol. 47, pp. 956–964, June 1999.

[29] S. March, "Phase velocity compensation in parallel-coupled microstrip," in *Microwave Symposium Digest, 1982 IEEE MTT-S International*, pp. 410–412, June 1982.

[30] S. Lee and Y. Lee, "A design method for microstrip directional couplers loaded with shunt inductors for directivity enhancement," *Microwave Theory and Techniques, IEEE Transactions on*, vol. 58, pp. 994–1002, Apr. 2010.

[31] J. Muller, M. Pham, and A. Jacob, "Directional coupler compensation with optimally positioned capacitances," *Microwave Theory and Techniques, IEEE Transactions on*, vol. 59, no. 11, pp. 2824–2832, 2011.

[32] Y. Wu, W. Sun, S.-W. Leung, Y. Diao, K.-H. Chan, and Y.-M. Siu, "Single-layer microstrip high-directivity coupled-line coupler with tight coupling," *Microwave Theory and Techniques, IEEE Transactions on*, vol. 61, no. 2, pp. 746–753, 2013.

[33] J. Muller and A. Jacob, "Complex compensation of coupled line structures in inhomogeneous media," in *Microwave Symposium Digest, 2008 IEEE MTT-S International*, pp. 1007–1010, June 2008.

[34] W.-K. Kim, M.-Q. Lee, J.-H. Kim, H. sun Lim, J.-W. Yu, B.-J. Jang, and J.-S. Park, "A passive circulator with high isolation using a directional coupler for RFID," in *Microwave Symposium Digest, 2006. IEEE MTT-S International*, pp. 1177–1180, June 2006.

[35] S. Bensmida and F. Ghannouchi, "New high directivity coupler design using feed-forward compensation technique," in *Microwave Conference, 2008. EuMC 2008. 38th European*, pp. 191–194, Oct. 2008.

[36] K. Yamauchi, A. Inoue, and M. Miyazaki, "High directivity quarter-wave microstrip coupler with cancellation circuit of Wilkinson divider," in *Microwave Conference, 2008. EuMC 2008. 38th European*, pp. 195–198, Oct. 2008.

[37] K. Yamamoto, H. Kurusu, S. Suzuki, and M. Miyashita, “High-directivity enhancement with passive and active bypass circuit techniques for GaAs MMIC microstrip directional couplers,” *Microwave Theory and Techniques, IEEE Transactions on*, vol. 59, pp. 3095–3107, Dec. 2011.

[38] V. Tas and A. Atalar, “Using phase relations in microstrip directional couplers to achieve high directivity,” *Microwave Theory and Techniques, IEEE Transactions on*, vol. 61, pp. 4063–4071, Dec 2013.

[39] V. Tas and A. Atalar, “An optimized isolation network for the wilkinson divider,” *Microwave Theory and Techniques, IEEE Transactions on*, vol. 62, pp. 3393–3402, Dec 2014.

[40] D. M. Pozar, *Microwave Engineering.* John Wiley and Sons, Inc., 1998.

[41] S. Horst, R. Bairavasubramanian, M. Tentzeris, and J. Papapolymerou, “Modified Wilkinson power dividers for millimeter-wave integrated circuits,” *IEEE Trans. Microw. Theory Techn.*, vol. 55, pp. 2439–2446, Nov. 2007.

[42] C. Trantanella, “A novel power divider with enhanced physical and electrical port isolation,” in *IEEE MTT-S Int. Microw. Symp. Dig.*, pp. 129–132, May 2010.

[43] X. Lan, P. Chang-Chien, F. Fong, D. Eaves, X. Zeng, and M. Kintis, “Ultra-wideband power divider using multi-wafer packaging technology,” *IEEE Microw. Compon. Lett.*, vol. 21, pp. 46–48, Jan. 2011.

[44] S.-H. Kim, J.-H. Yoon, Y. Kim, and Y.-C. Yoon, “A modified Wilkinson divider using zero-degree phase shifting composite right/left-handed transmission line,” in *IEEE MTT-S Int. Microw. Symp. Dig.*, pp. 1556–1559, May. 2010.

[45] X. Wang, I. Sakagami, A. Mase, and M. Ichimura, “Trantanella Wilkinson power divider with additional transmission lines for simple layout,” *IET Microw. Antennas Propag.*, vol. 8, pp. 666–672, June 2014.

[46] H.-R. Ahn and S. Nam, “3-db power dividers with equal complex termination impedances and design methods for controlling isolation circuits,” *IEEE Trans. Microw. Theory Techn.*, vol. 61, pp. 3872–3883, Nov. 2013.

[47] S. B. Cohn, “Optimum design of stepped transmission-line transformers,” *IRE Trans. Microw. Theory Techn.*, vol. 3, pp. 16–20, Apr. 1955.

[48] V. Tas and A. Atalar, “A performance enhanced power divider structure,” in *IEEE MTT-S Int. Microw. Symp. Dig.*, pp. 1–4, June 2014.

[49] R. E. Collin, *Foundations for Microwave Engineering.* McGraw-Hill Inc., 1992.

[50] M. Kirschning and R. Jansen, “Accurate wide-range design equations for the frequency-dependent characteristic of parallel coupled microstrip lines,” *Microwave Theory and Techniques, IEEE Transactions on*, vol. 32, no. 1, pp. 83–90, 1984.

[51] Y. Zhu, J. Zhang, H. Zhu, J. Cheng, and J. Li, “Compact microstrip line directional coupler with high directivity,” *J. of Electromagnetic waves and application*, vol. 26, no. 11-12, pp. 1619–1623, 2012.

[52] A. Eroglu and J. K. Lee, “The complete design of microstrip directional couplers using the synthesis technique,” *Instrumentation and Measurement, IEEE Transactions on*, vol. 57, pp. 2756–2761, Dec. 2008.

Appendix A

Phase Difference Analysis Using Network Theory

Network analysis yields that a reciprocal, lossless, matched four-port network is a directional coupler with infinite directivity [40]. Unfortunately, this is an idealized situation: For real life couplers the directivity is finite since the four-port matching constraint is not satisfied perfectly although the reciprocity condition is valid and the loss can be kept at very small values.

The lossless condition dictates the following relation between the S-parameters [40]

$$\sum_{k=1}^{4} S_{km}S_{kn}^{*} = \begin{cases} 1, & \text{if } m = n. \\ 0, & \text{otherwise.} \end{cases} \tag{A.1}$$

where * denotes the complex conjugate operation. Using Eq. (4.1) and (A.1), we find

$$|\Gamma|^2 + |T|^2 + |I|^2 + |C|^2 = 1 \tag{A.2}$$

$$\Gamma T^* + T\Gamma^* + CI^* + IC^* = 2(\mathscr{Re}\{\Gamma T^*\} + \mathscr{Re}\{CI^*\}) = 0 \tag{A.3}$$

$$\Gamma C^* + C\Gamma^* + TI^* + IT^* = 2(\mathscr{Re}\{\Gamma C^*\} + \mathscr{Re}\{TI^*\}) = 0 \tag{A.4}$$

$$\Gamma I^* + I\Gamma^* + TC^* + CT^* = 2(\mathscr{Re}\{\Gamma I^*\} + \mathscr{Re}\{TC^*\}) = 0 \tag{A.5}$$

where $\mathscr{Re}\{\}$ indicates the real part operation.

Let us consider a weakly coupled coupler with a coupling coefficient:

$$|C| \ll 1 \tag{A.6}$$

Obviously, the isolation coefficient is even smaller

$$|I| < |C| \ll 1 \tag{A.7}$$

If the coupler is designed to have a low reflection coefficient

$$|\Gamma| \ll 1 \tag{A.8}$$

From (A.2), (A.6), (A.7) and (A.8) we find

$$|T| \approx 1 \tag{A.9}$$

Using (A.7), (A.8) we find $\mathcal{Re}\{\Gamma I^*\} \approx 0$ is negligible. From (A.5) we must also have $\mathcal{Re}\{TC^*\} \approx 0$. Therefore,

$$\angle T - \angle C = \pm\pi/2 \tag{A.10}$$

which is a well known characteristic of the couplers. Using (A.9) and (A.10) we rewrite (A.3) and (A.4) as

$$\mp|\Gamma| \sin(\angle\Gamma - \angle C) + |I||C| \cos(\angle I - \angle C) = 0 \tag{A.11}$$

$$|\Gamma||C| \cos(\angle\Gamma - \angle C) \mp |I| \sin(\angle I - \angle C) = 0 \tag{A.12}$$

Rearranging these equations we get

$$\left(\frac{|I| \sin(\angle I - \angle C)}{|\Gamma||C|}\right)^2 + \left(\frac{|I||C| \cos(\angle I - \angle C)}{|\Gamma|}\right)^2 = 1 \tag{A.13}$$

Since $\cos^2(\angle I - \angle C) + \sin^2(\angle I - \angle C) = 1$ we arrive at

$$\angle I - \angle C = \tan^{-1}\sqrt{\frac{1 - |\frac{IC}{\Gamma}|^2}{|\frac{I}{\Gamma C}|^2 - 1}} \pm n\pi \tag{A.14}$$

For example, in a microstrip coupler with a directivity of 14dB, coupling of 20 dB and return loss of 30dB, the deviation of $\angle I - \angle C$ from $n\pi$ is less than 0.16 radians (9.4°). If the return loss is 40 dB, the deviation reduces to 0.05 radians (2.9°).